

Nanostructured Catalysts for the Electrochemical Reduction of CO₂

Ma, Ming; Smith, Wilson

Publication date

2017

Document Version

Final published version

Published in

Anisotropic and Shape-Selective Nanomaterials

Citation (APA)

Ma, M., & Smith, W. (2017). Nanostructured Catalysts for the Electrochemical Reduction of CO₂. In *Anisotropic and Shape-Selective Nanomaterials: Structure-Property Relationships* (pp. 337-373). (Nanostructure Science and Technology). Springer. https://doi.org/10.1007/978-3-319-59662-4_11

Important note

To cite this publication, please use the final published version (if applicable). Please check the document version above.

Copyright

Other than for strictly personal use, it is not permitted to download, forward or distribute the text or part of it, without the consent of the author(s) and/or copyright holder(s), unless the work is under an open content license such as Creative Commons.

Takedown policy

Please contact us and provide details if you believe this document breaches copyrights. We will remove access to the work immediately and investigate your claim.

Chapter 11

Nanostructured Catalysts for the Electrochemical Reduction of CO₂

Ming Ma and Wilson A. Smith

Abstract The electrochemical conversion of CO₂ into carbon-based fuels has attracted considerable attention as a promising strategy for closing the anthropogenic carbon cycle. A key challenge for achieving this goal is to develop selective, stable, and efficient electrocatalysts for the electrocatalytic reduction of CO₂. Nanostructured catalysts can provide many advantages compared to bulk materials, including the increase of active sites, the change of the local pH of the electrolyte, and improved stability. This chapter reviews the recent development of nanostructured metal catalysts for the electrocatalytic reduction of CO₂, mainly focusing on the fabrication, characterization, catalytic performance, and the reaction mechanism of these materials. In addition, the recent utilization of nanostructured bimetallic catalysts are introduced and a fundamental understanding of the reaction mechanism for their ability to reduce CO₂ is discussed. Finally, nanostructured carbon is shortly reviewed due to its low cost and improved catalytic activity and stability for the electroreduction of CO₂.

Keywords Electrochemical reduction of CO₂ · Conversion of CO₂ into fuels · Electrocatalysts · Metal nanocatalysts · Bimetallic nanocatalysts · Nano-carbon catalysts

M. Ma · W.A. Smith (✉)
Materials for Energy Conversion and Storage (MECS),
Department of Chemical Engineering, Faculty of Applied Sciences,
Delft University of Technology, 2629 HZ Delft, The Netherlands
e-mail: w.smith@tudelft.nl

© Springer International Publishing AG 2017
S.E. Hunyadi Murph et al. (eds.), *Anisotropic and Shape-Selective Nanomaterials*,
Nanostructure Science and Technology, DOI 10.1007/978-3-319-59662-4_11

337

11.1 Introduction

11.1.1 Background

The global atmospheric concentration of carbon dioxide (CO_2) has increased dramatically due to human activity, particularly after the industrial revolution. The accumulation of CO_2 (greenhouse gas) in the atmosphere is a serious environmental threat and a leading cause of global climate change [1, 2]. The increased global mean temperature may trigger the rise of sea level and the frequency and intensity of extreme weather events. In addition, the increase of the global CO_2 concentration has resulted in an increased ocean acidification, leading to the demise of many natural habitats and aquatic species [3, 4]. The oceans are a principal sink for dissolving the anthropogenic CO_2 where it is estimated to have caused a rise of 30% in the concentration of H^+ in the ocean surface waters since the early 1900s, which may adversely affect many marine ecosystems in the near future [4].

For mitigating the atmospheric CO_2 concentration, carbon capture and sequestration (CCS) at large emission sources such as industrial power plants has been proposed. However, there are some unknown ecological and environmental impacts and risks associated with the sequestration methods including geological and deep sea storage. Thus, carbon capture and utilization (CCU) could be a feasible strategy. For the utilization of the captured CO_2 , the electrochemical reduction of CO_2 to fuels and value-added chemicals at mild conditions has attracted considerable attention as a promising solution [5–10]. In this process, the captured CO_2 could be utilized as a chemical feedstock and converted into carbon monoxide (CO), methane (CH_4), ethylene (C_2H_4), and even liquid products such as formic acid (HCOOH), methanol (CH_3OH) and ethanol ($\text{C}_2\text{H}_5\text{OH}$) [9–11]. The high energy density hydrocarbons can be directly and conveniently utilized as fuels within the current energy infrastructure. In addition, the production of CO is very interesting since it can be used as a reagent in the Fischer–Tropsch process, a well-developed technology that has been widely used in industry to convert syngas (CO and hydrogen (H_2)) into valuable chemicals such as methanol and synthetic fuels (such as diesel fuel) [5, 6].

In order to avoid extra CO_2 emission, the electrochemical reduction of CO_2 should be powered by electricity from renewable energy sources such as solar energy, hydropower and wind energy [6, 9]. In this way, the anthropogenic carbon cycle can be closed by the conversion of CO_2 into fuels and useful products (Fig. 11.1). A key technological challenge for achieving this goal is to develop cheap and earth-abundant catalysts that are capable of electrochemically reducing CO_2 in cost-effective process with high efficiency, controllable selectivity and long-term stability [5, 9, 12–14].

Hori and other researchers have investigated the electrocatalytic reduction of CO_2 using various metal foil electrodes in CO_2 -saturated aqueous solutions [8, 9, 15–20]. Recent studies indicate that a nanostructured metal catalyst has a significant effect on the catalytic selectivity, efficiency and stability in the electrochemical reduction of CO_2 [14, 21–24].

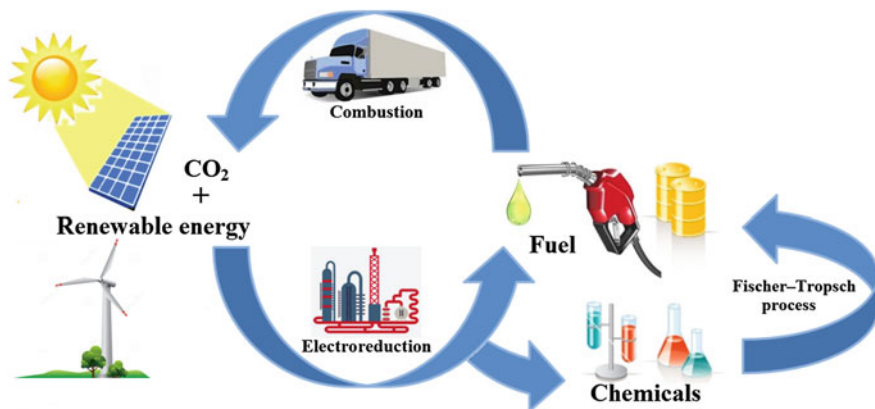
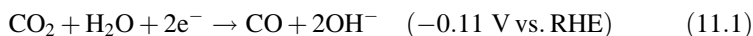


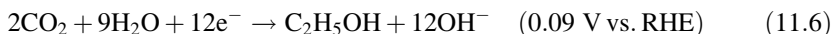
Fig. 11.1 The carbon-neutral fuel production from the electrochemical reduction of CO₂ coupled to renewable energy sources such as solar energy, wind energy and hydropower, offers a promising route to close the anthropogenic carbon cycle

A review of nanostructured catalysts for the electrocatalytic reduction of CO₂ is presented in this chapter, mainly focusing on the fabrication, characterization and catalytic performance of the nanostructured metal catalysts. In addition, a fundamental understanding of the reaction mechanism for the electrochemical CO₂ reduction on nanomaterial-based catalysts is also introduced.

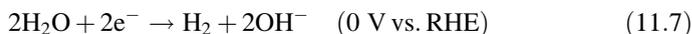
11.1.2 Bulk Metal Catalysts for CO₂ Reduction

In the electrocatalytic CO₂ reduction process, CO₂ can be converted into many different products when combined with water on metal surfaces, and each product is formed by a different number of electrons at different equilibrium potentials. The electrochemical reduction of CO₂ to CO, CH₄, C₂H₄, HCOOH, CH₃OH and C₂H₅OH with their corresponding equilibrium potentials (with respect to the reversible hydrogen electrode (RHE)) are given in the following reaction equations:





H_2 evolution is a competing reaction with CO_2 reduction in CO_2 -saturated electrolytes. Thus, water could be reduced to H_2 during the CO_2 reduction according to the below reaction:



It is important to note two key insights from the aforementioned reaction equations. Firstly, the thermodynamic potential for each product formation are very close to that of hydrogen (0 V vs. RHE), which indicates that it theoretically should not add a substantial amount of extra potential to drive these reactions compared to simple water reduction. However, it is also important to understand that many of these reactions require many electron (and proton coupled electron) transfer steps, as shown by the number of electrons needed to drive each reaction (Eqs. 11.1–11.7). Secondly, the number of electrons required to form certain product generally scales with the increased amount of reaction intermediates, and thus the activation energy for each intermediate needs to be overcome to form the final product. Therefore, while the overall thermodynamic potential for each product formation seems to be small and reasonable, the formation of many intermediates and electron transfer could significantly increase overpotentials, and the overpotential of ~ 1 V is generally needed to drive each reaction effectively and selectively in many practical cases. The actual required overpotentials for driving the reduction of CO_2 are strongly materials dependent.

Hori and coworkers carried out the electrochemical CO_2 reduction over various transition metal electrodes (Table 11.1), discovering several metallic electrocatalyst materials with the capability of reducing CO_2 [8]. It has been demonstrated that polycrystalline Ag and Zn show relatively high faradaic efficiency (FE) for the electrocatalytic reduction of CO_2 to CO, although these occur at high overpotentials. In addition, Au is the most efficient and selective metal surface for the electrocatalytic conversion of CO_2 into CO at a moderate overpotential, as presented in Table 11.1. Further reduction of CO to more complex products is rare on Au, Ag and Zn catalysts due to the weak binding strength of CO with these metallic surface [11, 25]. However, the strong binding of CO on Ni, Pt and Fe metallic catalysts limits the desorption of CO, [11, 25] resulting in suppressed CO_2 reduction with dominant H_2 evolution, as shown in Table 11.1. Among the identified transition metal materials, copper electrodes can uniquely reduce CO_2 to CH_4 , C_2H_4 , and alcohols at significant amounts in CO_2 -saturated aqueous electrolytes at ambient pressure and temperature [15, 26].

The synthesis of products from CO_2 on metal catalysts is a complex multistep reaction with multiple adsorbed intermediates, most notably adsorbed CO [10, 27, 28]. The reaction mechanisms for the various products are attributed to the adsorption strength of intermediates (such as CO, COH, CHO and CH_3) on the

Table 11.1 Faradaic efficiencies of products in CO₂ reduction at various metal electrodes. Electrolyte: CO₂-saturated 0.1 M KHCO₃, T = 18.5 ± 0.5 °C. Reprinted with permission from Ref. [8]

Electrode	V versus SHE	Faradaic efficiency (%)							
		CH ₄	C ₂ H ₄	Ethanol	n-propanol	CO	HCOOH	H ₂	Total
Au	-1.14	0	0	0	0	87.1	0.7	10.2	98.0
Ag	-1.37	0	0	0	0	81.5	0.8	12.4	94.6
Zn	-1.54	0	0	0	0	79.4	6.1	9.9	95.4
Pd	-1.20	2.9	0	0	0	28.3	2.8	26.2	60.2
Ga	-1.24	0	0	0	0	23.2	0	79.0	102.0
Pb	-1.63	0	0	0	0	0	97.4	5.0	102.4
Hg	-1.51	0	0	0	0	0	99.5	0	99.5
Tl	-1.60	0	0	0	0	0	95.1	6.2	101.3
In	-1.55	0	0	0	0	2.1	94.9	3.3	100.3
Sn	-1.48	0	0	0	0	7.1	88.4	4.6	100.1
Cd	-1.63	1.3	0	0	0	13.9	78.4	9.4	103.0
Bi	-1.56	–	–	–	–	–	77	0	–
Cu	-1.44	33.3	25.5	5.7	3.0	1.3	9.4	20.5	103.5
Ni	-1.48	1.8	0.1	0	0	0	1.4	88.9	92.4
Fe	-0.91	0	0	0	0	0	0	94.8	94.8
Pt	-1.07	0	0	0	0	0	0.1	95.7	95.8
Ti	-1.60	0	0	0	0	0	0	99.7	99.7

catalyst surface during the electrochemical reduction of CO₂ [24, 29, 30]. The catalyst provides the reactive sites, and the product selectivity in the electrocatalytic reduction of CO₂ is affected by whether the reactants and other related species are adsorbed at the active sites.

Because H₂ evolution is always a competing reaction with CO₂ reduction in CO₂-saturated electrolytes, H₂ was also identified and quantified during CO₂ reduction electrolysis. Polycrystalline Pt, Ni and Fe, shown in the Table 11.1, exhibit an extremely high selectivity for H₂ (water reduction is always a competing reaction) along with very little catalytic activity for the electrochemical reduction of CO₂. On Pt, Ni and Fe, it is easy for CO₂ activation and conversion of CO₂ into adsorbed CO, but the rate determining step for CO generation is the desorption of CO due to the strong binding of CO on the catalyst surface [11, 25, 31]. The coverage of CO adsorbed on polycrystalline Pt, Ni and Fe blocks the reactive sites for CO₂ reduction, influencing the catalytic activity for the electrocatalytic reduction of CO₂. Recently, the catalytic activity and selectivity for the electroreduction of CO₂ on seven transition metal surfaces (Au, Ag, Zn, Cu, Ni, Pt and Fe) were further investigated by Jaramillo [9, 32]. Au, Ag and Zn exhibit a high faradaic efficiency for the reduction of CO₂ to CO due to the surface of Au, Ag and Zn bind CO weakly, while Ni, Pt, and Fe with binding CO strongly have a very low catalytic activity for CO₂ reduction along with dominant H₂ evolution. Cu, with a moderate CO binding energy, uniquely shows a total of 16 different CO₂ reduction products [9].

11.1.3 Nanostructured Metal Catalysts for CO₂ Reduction

Catalytic behavior is not only strongly materials-dependent, but also extremely morphology-dependent [33]. The development of nanoscience research provides the opportunity to synthesize nanocatalysts with controllable size and shape, which has led to the discovery of the altered or enhanced catalytic activity and selectivity with the size and shape of nanostructured catalyst. Researchers have demonstrated that a nanostructured catalyst can exhibit very different behavior compared to its bulk counterpart. Much work in the field has focused on the elucidation of the effects of nanostructured catalysts.

Recently nanostructured metallic catalysts have been the object of an increasing interest for the electrocatalytic reduction of CO₂. The main advantage of metallic nanocatalysts is that nanostructured catalysts are capable of providing more active sites on the high surface area compared to bulk metal catalysts. The increased active surface sites on nanocatalysts may cause an enhanced catalytic performance due to the fact that the catalytic activity is proportional to the number of the active surface sites [34]. In addition, the morphology of nanostructured surface contains more low-coordinated sites (such as edge sites and corner sites) that are more active for CO₂ reduction in comparison with smooth or planar surface [35]. Furthermore, the catalytic stability of the electrochemical reduction of CO₂ has been improved on nanostructured catalysts, which can be attributed to the enhanced tolerance to heavy metal impurities in an electrolyte. Hori has demonstrated that unavoidable ppm concentration of heavy metal impurities (such as Fe or Pb) in the electrolytes can be reduced and deposited on the cathodic electrode surface, which could poison a flat catalyst, resulting in a significant influence in the electrocatalytic activity for CO₂ reduction [8]. The large surface area of nanostructured electrocatalysts could adapt the contamination or impurities, having a better catalytic stability [34].

This chapter mainly focuses on the recent development of heterogeneous nanocatalysts for the electrochemical reduction of CO₂, including the fabrication, characterization, catalytic performance and reaction mechanism of nanostructured metallic catalysts.

11.2 Nanostructured Metal Catalysts for CO₂ Reduction to CO

The selective conversion of CO₂ into CO is a promising route for clean energy generation. CO can be used as feedstock in the Fischer–Tropsch process, a well-developed technology that has been used in industry to produce chemicals (such as methanol) and synthetic fuels (such as diesel fuel) from syngas (CO + H₂) for many decades [5, 6]. While several electrocatalyst materials (such as Au, Ag and Zn) are capable of reducing CO₂ to CO in CO₂-saturated aqueous solutions at ambient temperature and pressure, all suffer from one or more of the following problems: high overpotential requirement, low current density and rapid

deactivation of CO₂ reduction activity in favor of H₂ evolution [8, 13, 17]. The main challenge for the electrochemical syngas production is the development of electrocatalysts that are capable of reducing CO₂ to CO efficiently and selectively at low overpotential over a long period of time.

11.2.1 Nanostructured Au

Au is currently the most efficient electrocatalytic surface for the reduction of CO₂ to CO (Table 11.1). It has been demonstrated that polycrystalline Au is capable of reducing CO₂ to CO with a high faradaic efficiency of ~87% at -0.74 versus RHE [32]. While the low abundance and high cost of Au may prevent its large-scale applications, it remains an interesting catalytic material for fundamental investigation due to a high selectivity for CO formation at a relatively low overpotential in the electroreduction of CO₂ (Table 11.1).

11.2.1.1 Au Nanoparticles

Min et al. reported the electrocatalytic CO₂ conversion into CO by nanostructured gold catalysts deposited on carbon papers by an e-beam evaporator using an Au pellet (99.99%) source [36]. The morphology of the deposited Au was observed to vary from the small nanoparticles (NPs) to aggregated clusters to layered film (Fig. 11.2).

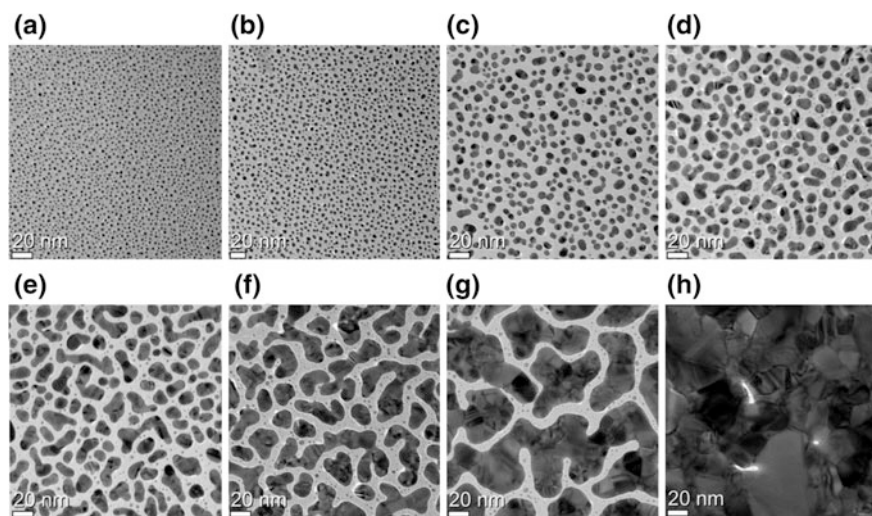


Fig. 11.2 TEM images of Au samples, showing the morphology changes with the dependence of Au coverages which were presented by Au film thickness (increased Au coverages from **a** to **h**). Reprinted with permission from Ref. [36]

The CO faradaic efficiency and production rate were found to increase with increasing the Au amount. The FE for CO formation reached the saturation point at samples thicker than Au-4 (Au-4 represents that Au amount corresponds to 4 nm thick Au film), which is comparable with a commercial Au foil. In addition, Nam et al. synthesized a concave rhombic dodecahedron (RD) gold nanoparticle by using 4-aminothiophenol as an additive and demonstrated that this concave RD had a superior electrocatalytic performance for reduction CO₂ to CO in CO₂-saturated aqueous solutions [37]. For instance, concave RD achieved a FE of approximately 52% for CO formation at a potential of -0.26 V versus RHE, which corresponds to an overpotential of 0.15 V relative to the CO₂/CO equilibrium potential (-0.11 V vs. RHE).

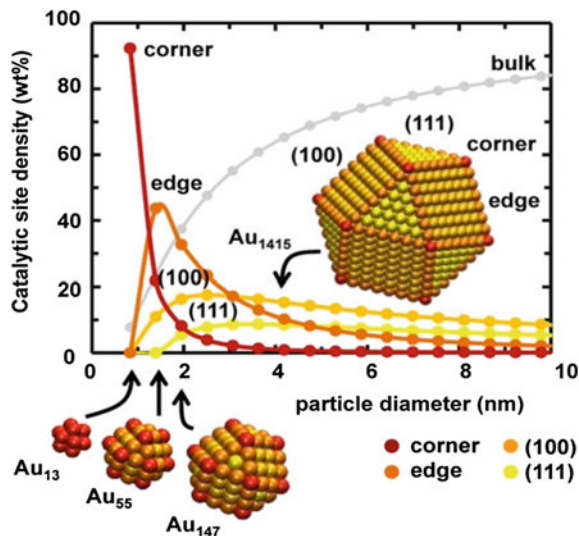
Au clusters have also been explored by the combination of experimental and computational studies, providing insights into the electronic interactions between Au₂₅ clusters and weakly bound adsorbates [38]. It was discovered that the Au₂₅ clusters could perform as superior catalysts for the electrochemical conversion of CO₂ into CO and promote the reduction of CO₂ to CO within 90 mV of the formal potential (thermodynamic limit), which represents an approximate 200–300 mV reduction in potential compared to the larger Au NPs and bulk Au tested.

Recently, Sun et al. reported that the electrocatalytic reduction of CO₂ on Au NPs with a series of sizes (4, 6, 8 and 10 nm) in CO₂-saturated 0.5 M KHCO₃ [39]. The crystallite diameters of 4, 6, 8 and 10 nm NPs were estimated to be 2.0, 2.3, 4.0 and 5.9 nm, respectively. Among 4, 6, 8 and 10 nm Au NPs, the 8 nm NPs exhibited the highest selectivity for the reduction of CO₂ to CO (FE = 90% at -0.67 V vs. RHE). Density functional theory (DFT) calculations on different crystalline faces suggested that edge sites on Au NPs are active for CO formation while corner sites favor the competitive H₂ evolution reaction. To understand the size-dependent electroreduction of CO₂ on Au NPs, the correlation of the density of catalytically active surface sites with the cluster diameter was investigated, as shown in Fig. 11.3. It was found that more edge sites than corner sites on the Au NP surface could facilitate the stabilization of COOH[•] intermediate, resulting in the improved reduction of CO₂ to CO with suppressed H₂ evolution.

11.2.1.2 Au Nanowires

The previous study on monodispersed Au NPs indicated that the edge sites of Au NPs are favorable for the reduction CO₂ to CO while corner sites are active for the H₂ evolution [39]. Thus, a one-dimensional morphology may offer an abundance of edge sites which is preferred for the reduction of CO₂. Zhu et al. demonstrated ultrathin Au nanowires (NWs) for the selective electrochemical reduction of CO₂ to CO [40]. A facile seed-mediated growth method was developed to fabricate the ultrathin Au NWs by reducing HAuCl₄ in the presence of 2 nm nanoparticles.

Fig. 11.3 Density of adsorption sites (yellow, light orange, dark orange, or red symbols for (111), (001), edge, or corner on-top sites, respectively) on closed-shell cuboctahedral Au clusters versus the cluster diameter. The weight fraction of Au bulk atoms is marked with gray dots. Reprinted with permission from Ref. [39]

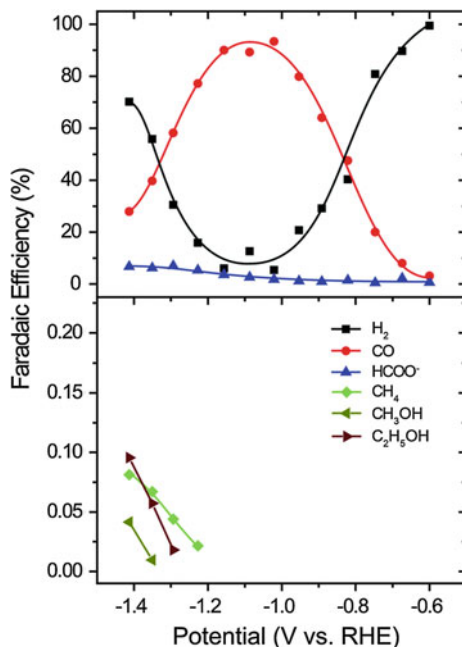


These Au NWs are capable of catalyzing CO₂ to form CO with FE of 94% at -0.35 V versus RHE in CO₂-saturated 0.5 M KHCO₃. The modeling work (DFT) revealed that the excellent catalytic performance for the reduction of CO₂ to CO on Au NWs is ascribed to a high edge-to-corner ratio in ultrathin Au NWs and the weak CO binding on these reactive edge sites.

11.2.2 Nanostructured Ag

Metallic Ag has attracted considerable attention due to its relatively low cost compared to Au, and its high selectivity for the conversion of CO₂ into CO [8, 11]. As presented in Table 11.1, Ag foils are capable of electrochemically reducing CO₂ to CO with a high FE at a relatively smaller overpotential than other metallic counterparts (except for Au). Recently, Jaramillo investigated the catalytic activity and selectivity of the electrochemical reduction of CO₂ as a function of potential on metallic silver surfaces under ambient conditions [20]. The authors found that the applied potential can significantly influence the selectivity for the two major products (CO and H₂). Specifically, the optimal selectivity for CO formation on the polycrystalline silver catalyst was observed at the range from -1.0 to -1.2 V versus RHE and hydrogen evolution dominated at very high and low potentials (Fig. 11.4). By using high sensitivity of the experimental methods for identifying and quantifying products of CO₂ reduction, formate, methane, methanol, and ethanol were observed as minor products (methanol and ethanol formation had never been reported on Ag before this study).

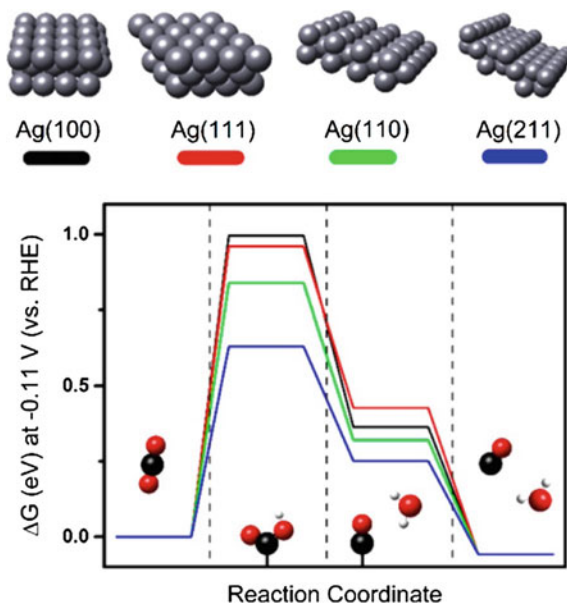
Fig. 11.4 Faradaic efficiency for each product as a function of potential on polycrystalline Ag foils. Reprinted with permission from Ref. [20]



On Ag catalysts, the overpotential (>0.9 V) required for driving the electrocatalytic reduction of CO_2 efficiently and selectively with suppressed H_2O reduction remains relatively high [32]. The large overpotential required for the reduction of CO_2 is attributed to the hindrance for the initial electron transfer to a CO_2 molecule to form a $\text{CO}_2^{\cdot-}$ or COOH^{\cdot} intermediate [5, 12, 25, 35]. Nanostructured Ag catalysts have been considered to be a promising candidate for the electroreduction of CO_2 to CO. It has been demonstrated that the surface of nanostructured Ag catalysts offers the low-coordinated surface Ag sites, which is favorable for CO_2 fixation (to stabilize the formed COOH^{\cdot} intermediate) through reducing the activation energy barrier of the initial electron transfer [35].

In addition, Hori et al. has investigated the electroreduction of CO_2 on single crystalline silver electrodes, showing that the CO_2 conversion into CO is favorable on Ag(110) compared to Ag(111) or Ag(100) [17]. Recently, a DFT simulation study (Fig. 11.5) exhibited that Ag(110) or Ag(211) surface has a lower free energy change for the first proton-coupled electron transfer for COOH^{\cdot} stabilization than Ag(111) or Ag(100), resulting in better catalytic activity for the reduction of CO_2 to CO on Ag(110) or Ag(211) [35]. It was believed that stepped Ag(110) or Ag(211) surfaces are much prevalent on the nanostructured Ag catalysts than that on bulk Ag electrodes [35].

Fig. 11.5 Free energy diagrams for the electrochemical reduction of CO₂ to CO on flat (Ag(100) and Ag(111)) and edge (Ag(221) and Ag(110)) surfaces. The first two steps include a simultaneous proton/electron transfer, with the final molecular surface configuration at each step depicted on the *bottom* of the graph. Values of ΔG are reported with an applied potential of -0.11 V versus RHE. Sphere colors: *white*, H; *black*, C; *red*, O; *silver*, Ag. Reprinted with permission from Ref. [35]



11.2.2.1 Ag Nanoparticles

Recently Kim et al. have examined silver nanoparticles with different sizes for the electrocatalytic reduction of CO₂ in CO₂-saturated 0.5 M KHCO₃ [41]. Silver nanoparticles with three different sizes (3, 5 and 10 nm) were fabricated on carbon substrates, respectively, by a facile one-pot method using cysteamine as an anchoring agent. The authors discovered that immobilized Ag nanoparticles supported on carbon had an increased FE and a lower overpotential for selective reduction of CO₂ to CO. Notably, the particle size of 5 nm exhibited the highest catalytic activity for the selective reduction of CO₂ to CO. As shown in Fig. 11.6b, a FE of 84.4% for CO formation and a decrease of the overpotential by 300 mV were observed on NPs with diameter of 5 nm at -0.75 V versus RHE compared to polycrystalline Ag foils. The DFT studies suggested that the specific interaction (Ag-S interaction) between Ag nanoparticles and the anchoring agents modified the catalyst induces a selectively higher affinity to the COOH⁻ intermediate, which effectively lowers the overpotential and improves the catalytic activity for the reduction of CO₂ to CO. In addition, for identifying the carbon source for the CO₂ reduction, a ¹³CO₂ isotope experiment was performed, which confirmed that the carbon source for CO formation was completely derived from the dissolved CO₂ in electrolytes, and carbon from carbon support or cysteamine were not involved in the reduction reaction.

A previous report also evaluated the Ag NP size effect, suggesting that the catalytic activity increases with decreasing particle size until a certain particle size

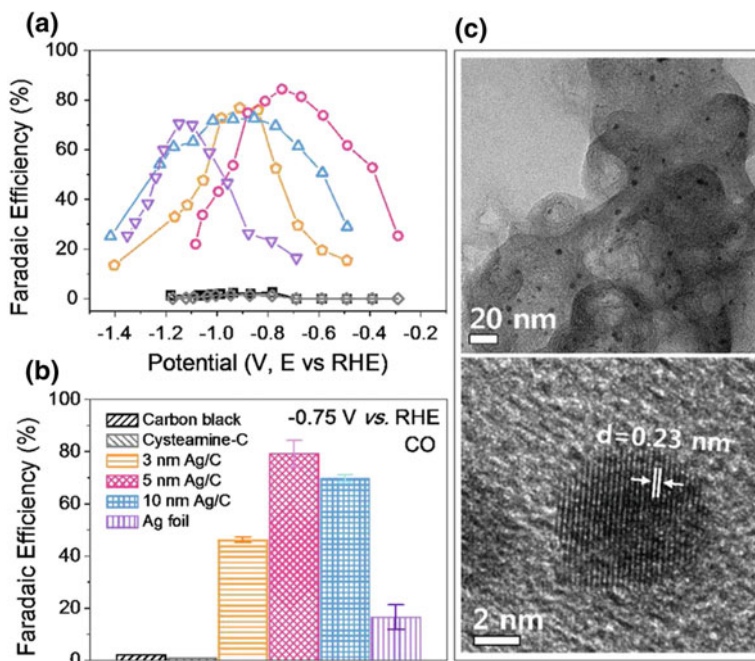


Fig. 11.6 CO faradaic efficiency **a** depending on applied potential and **b** fixed potential at -0.75 V (vs. RHE). CO₂ electrochemical reduction was performed in CO₂-saturated 0.5 M KHCO₃. **c** TEM image and HR-TEM image of 5 nm Ag/C after CO₂ reduction. Reprinted with permission from Ref. [41]

of 5 nm, and that the activity decreases with going to even smaller nanoparticle size (1 nm) [42]. This observation is consistent with the results from Kim (5 nm NPs offer the maximum catalytic activity for CO₂ reduction) [41].

11.2.2.2 Nanoporous Ag

Lu et al. reported that a nanoporous Ag catalyst prepared by the de-alloying of an Ag-Al precursor is capable of reducing CO₂ electrochemically to CO with a high FE of >90% at a moderate potential of -0.6 V versus RHE in CO₂-saturated 0.5 M KHCO₃ [5]. To explore the electrokinetics of CO₂ reduction, Tafel analysis was performed on the nanoporous Ag catalysts and the polycrystalline Ag electrode, respectively.

It is known that a two electron-transfer process is involved in the electroreduction of CO₂ to CO on Ag catalysts. Firstly, one electron is transferred to a CO₂ molecule to produce a CO₂⁻ intermediate, and then one proton is coupled to form a COOH⁻ intermediate. Subsequently, the COOH⁻ intermediate takes another electron and one proton, resulting in the CO formation on catalyst surface. The initial

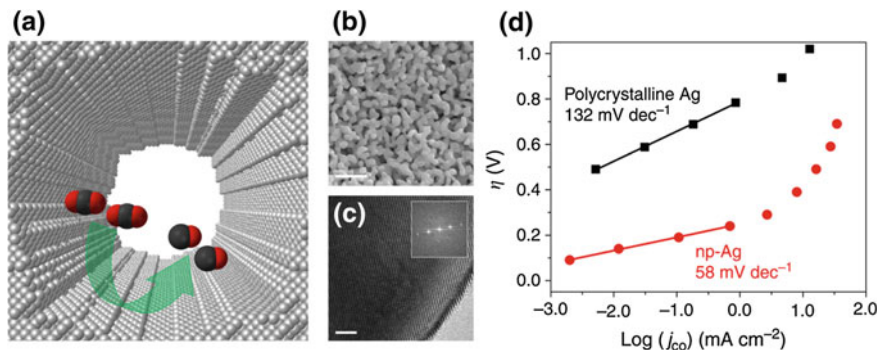


Fig. 11.7 **a** A schematic diagram of a nanopore of the silver electrocatalyst with highly curved internal surface. **b** Scanning electron micrograph of np-Ag dealloyed in 5 wt% HCl for 15 min and further in 1 wt% HCl for 30 min (scale bar, 500 nm). **c** Corresponding high-resolution transmission electron micrograph with visible lattice fringes. Inset: the Fourier transform shows that the np-Ag is composed of an extended crystalline network (scale bar, 2 nm). **d** Tafel plots of the partial current density for CO production. Reprinted with permission from Ref. [5]

electron transfer to a CO₂ molecule is the rate determining step for the overall process because the first electron transfer requires a much more negative potential compared to the following steps [5, 12, 25, 35]. A Tafel slope of 132 mV/dec for polycrystalline Ag shown in Fig. 11.7d indicates the rate determining step is the initial electron transfer to CO₂ for the formation of the CO₂⁻ adsorbed on polycrystalline Ag. In contrast, the nanoporous Ag with a Tafel slope of 58 mV/dec reveals a fast initial electron-transfer step, suggesting that a better stabilization for CO₂⁻ intermediate on nanoporous-Ag in comparison to the polycrystalline Ag. This study directly shows a clear advantage of CO₂ reduction catalysis on nanostructured electrodes.

11.2.3 Nanostructured Zn

Zn is an earth-abundant material, which is roughly 3 orders of magnitude more abundant in the Earth's crust than Ag. Hori et al. reported that polycrystalline Zn electrodes are capable of catalytically reducing CO₂ to CO with a FE of 79.4% [8]. However, the Zn electrodes require a relatively higher overpotential for driving CO₂ reduction selectively compared to Au and Ag (Table 11.1).

Nanostructured Zn dendrite electrodes were synthesized on Zn foil electrodes using an electrochemical Zn deposition [43]. As shown in Fig. 11.8a, the scanning electron microscope (SEM) images reveal that the dendrite layer was about 50–100 μm thick and uniformly deposited on Zn foils. The X-ray diffraction

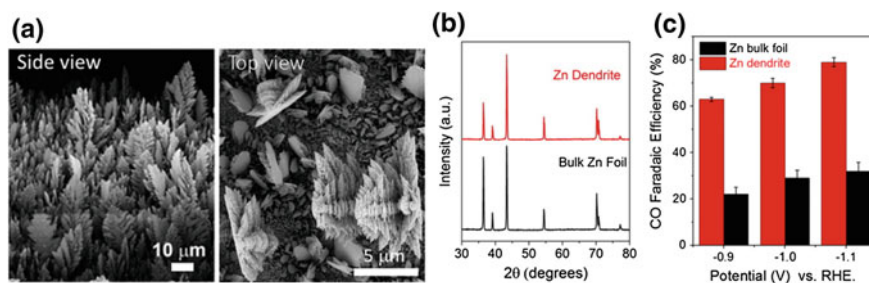


Fig. 11.8 **a** Typical SEM image for a Zn dendrite catalyst. **b** PXRD patterns of bulk and dendritic Zn electrodes. **c** CO faradaic efficiency for bulk and dendritic Zn electrocatalysts. Reprinted with permission from Ref. [43]

(XRD) patterns in Fig. 11.8b show that all the diffraction peaks of the nanostructured Zn dendrite and the Zn bulk foil are aligned precisely, indicating a pure metallic Zn. This nanostructured Zn dendrite catalyst was able to electrochemically reduce CO_2 to CO in an aqueous bicarbonate electrolyte, with a CO faradaic efficiency of around 3-fold higher than that of bulk Zn counterparts, as displayed in Fig. 11.8c.

11.2.4 Nanostructured Pd

Bao et al. investigated a particle size dependence for the electrocatalytic reduction of CO_2 on Pd NPs with the size range from 2.4 to 10.3 nm [44]. The authors discovered that an increase in the selectivity for CO production with reducing the size of Pd NPs, which varies from the FE of 5.8% on 10.3 nm Pd NPs to that of 91.2% on 3.7 nm NPs at -0.89 V versus RHE. DFT calculations suggested that corner and edge sites on small Pd NPs facilitate the adsorption of CO_2 and the stabilization of COOH^\cdot intermediates during CO_2 reduction compared with terrace one on large Pd NPs.

11.2.5 Metal Organic Frameworks

Metal Organic Frameworks (MOFs) have backbones constructed from metals and organic ligands, which are structured and porous materials with nano-scale pores for heterogeneous and homogeneous catalysis [45, 46]. Fe-based MOF catalysts have been recently used for the electrochemical reduction of CO_2 to CO (faradaic efficiencies are 41 ± 8 and $60 \pm 4\%$ for CO and H_2) [47]. The well-defined nanoscale porosity of the MOF facilitates access of the solvent, reactant, and electrolyte to the surface of catalytically active sites.

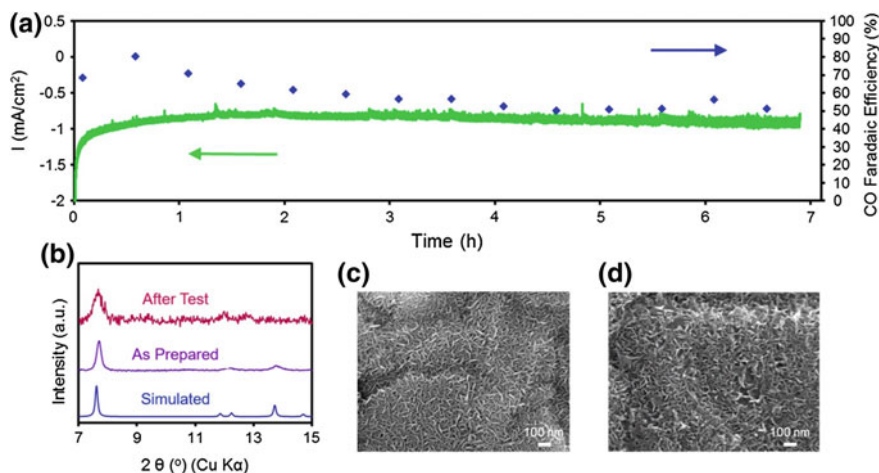


Fig. 11.9 Stability of the MOF catalyst is evaluated through chronoamperometric measurements in combination with faradaic efficiency measurements (a). XRD analysis indicates that the MOF retains its crystalline structure after chronoamperometric measurement (b). SEM images of the MOF catalyst film before (c) and after electrolysis (d) reveal the retention of the platelike morphology. Reprinted with permission from Ref. [46]

Yang et al. reported an efficient and selective nano-scale MOFs catalyst for the electrochemical generation of CO from CO₂ in CO₂-saturated aqueous bicarbonate solutions [46]. A cobalt-porphyrin MOF, Al₂(OH)₂TCPP-Co (TCPP-H2 = 4,4',4'',4'''-(porphyrin-5,10,15,20-tetrayl)tetrabenzoate) exhibited a FE of exceeding 76% for CO formation at -0.7 V versus RHE and a stable current of MOF catalysts was observed after initial electrolysis, as presented in Fig. 11.9a. The crystallinity of the MOF catalyst was still maintained after CO₂ reduction electrolysis (Fig. 11.9b) and the SEM images show that the retention of the platelike morphology after CO₂ reduction (Fig. 11.9c, d).

11.3 Nanostructured Metal Catalysts for CO₂ Reduction to Hydrocarbons

The conversion of CO₂ and H₂O into hydrocarbons on electrocatalysts has attracted considerable attention [9, 13, 14, 21]. The main advantages of directly forming hydrocarbons are their high energy density and the ease of utilization as fuels in our existing energy infrastructure. However, a major challenge of this goal is to develop electrocatalysts that are capable of reducing CO₂ efficiently and selectively at low potentials. Hori and his coworkers carried out CO₂ reduction over various metal electrodes (Table 11.1), and it was demonstrated that many electrocatalyst materials such as polycrystalline Cu, Au, Ag and Zn show high faradaic efficiency for the

electrochemical reduction of CO_2 , although these occur at very high overpotentials [8]. It was found that copper electrodes can uniquely reduce CO_2 to significant amounts of CH_4 , C_2H_4 , and alcohols in aqueous electrolytes at ambient pressure and temperature [8, 15, 26]. One main reason for this unique catalytic activity of copper is attributed to the appropriate binding strength of intermediates (such as CO , COH , CHO and CH_3 .) on the copper surface during the electrochemical reduction of CO_2 [24, 29, 30].

Recently, Jaramillo et al. [9] reported new insights into the electrocatalytic reduction of CO_2 on metallic Cu surface, finding as many as 16 different products from the electroreduction of CO_2 (five of them have never been reported previously). At low negative potential of > -0.75 V versus RHE, only H_2 , CO and HCOOH were detected on Cu. At -0.75 V versus RHE, C_2H_4 and CH_4 formation started to be observed. In addition, other C_2 and C_3 products were initially detectable at -0.95 V versus RHE.

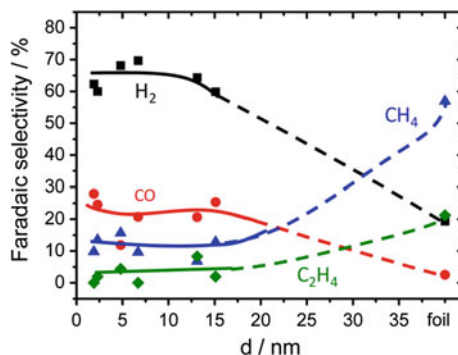
Hori et al. [48] investigated the electrochemical reduction of CO_2 on Cu single crystal electrodes (100), (110), and (111) in aqueous electrolytes at ambient pressure, showing that C_2H_4 is favorably produced on Cu(100) and CH_4 is preferred on Cu(111). In addition, the similar product selectivity was also observed for the electroreduction of CO on Cu single crystal electrodes [48, 49], due to the fact that CO is the intermediate in the reduction of CO_2 to hydrocarbons [29, 30, 50, 51]. Furthermore, a more detailed study on the effect of Cu crystal faces were carried out [18, 52].

Until now, copper is the only known material which is capable of catalyzing the formation of significant amounts of hydrocarbons at high reaction rates in aqueous solutions at ambient conditions of temperature and pressure [9, 22, 50]. However, controlling the product selectivity of the CO_2 reduction effectively at low overpotential with high current density for the formation of hydrocarbons is a major scientific challenge for the practical use of this technology [12–14, 53]. It has been demonstrated that the surface morphology and roughness of copper electrodes have a dramatic influence on the catalytic activity and product selectivity for the electrochemical reduction of CO_2 in an aqueous solution [14, 21–24].

11.3.1 *Cu Nanoparticles*

Tang et al. reported that Cu nanoparticle covered electrodes exhibited a better selectivity towards C_2H_4 and CO formation in comparison with an electropolished Cu electrode and an argon gas sputtered Cu electrode [24]. In that study, the increased catalytic selectivity for C_2H_4 formation in CO_2 reduction was explained by the roughened Cu surface which was able to provide a greater abundance of undercoordinated sites. In addition, Alivisatos et al. has demonstrated that Cu NPs supported on glassy carbon (n-Cu/C) exhibited a 4-fold higher methanation current densities compared to the high-purity Cu foil counterpart [54]. A faradaic efficiency of 80% for CH_4 was achieved on the n-Cu/C electrocatalysts. The rate-limiting step

Fig. 11.10 Catalytic selectivity of reaction products during the CO₂ electroreduction on Cu NPs in CO₂-saturated 0.1 M KHCO₃ at -1.1 V versus RHE under 25 °C. Reprinted with permission from Ref. [21]



for CH₄ on Cu foils is a single electron transfer to CO₂, which corresponds to a Tafel slope of 120 mV/dec. The Tafel slope for CH₄ is 60 ± 4.2 mV/dec on the n-Cu/C, which is consistent with the theoretical value of 59 mV/dec, indicating a one-electron pre-equilibrium step prior to a rate-determining non-electrochemical step.

Recently, the particle size dependence for the electrochemical reduction of CO₂ has been investigated on Cu NPs with the size range from 2 to 15 nm [21]. Cu NPs exhibited that an increase in the catalytic activity and selectivity for CO and H₂ with decreasing Cu particle size, as presented in Fig. 11.10. In addition, catalytic selectivity for hydrocarbons (CH₄ and C₂H₄) was suppressed on the nanoscale Cu surface compared to the bulk Cu foil. To gain insight into the Cu particle size effect, the atomic coordination of model spherical Cu particles from 1 to 18 nm was utilized, suggesting low-coordinated sites and the strong chemisorption are linked to the acceleration for H₂ evolution and the CO₂ reduction to CO.

11.3.2 Cu Nanowires

Smith et al. reported a new synthesis method to prepare a Cu nanowire catalyst for the electroreduction of CO₂ at room temperature and atmospheric pressure [55]. Cu nanowire array electrodes were synthesized through a two-step synthesis of Cu(OH)₂ and CuO nanowire arrays on Cu foil substrates and a subsequent electrochemical reduction of the CuO nanowire arrays. Cu(OH)₂ nanowire arrays (Fig. 11.11a) were first synthesized on Cu foils using a simple wet chemical method [56, 57]. After this step, CuO nanowire arrays were formed by annealing the Cu(OH)₂ nanowires at 150 °C for 2 h in an air atmosphere [55]. The resulting CuO nanowire arrays were directly utilized in the electrochemical reduction of CO₂ in CO₂-saturated 0.1 M KHCO₃ electrolytes, and were reduced to Cu nanowire during electrolysis. The CuO-derived Cu nanowire arrays are able to electrochemically reduce CO₂ to CO with a FE of ~50% at a moderate overpotential of 490 mV, which is significantly higher than that of polycrystalline Cu foil catalysts at identical

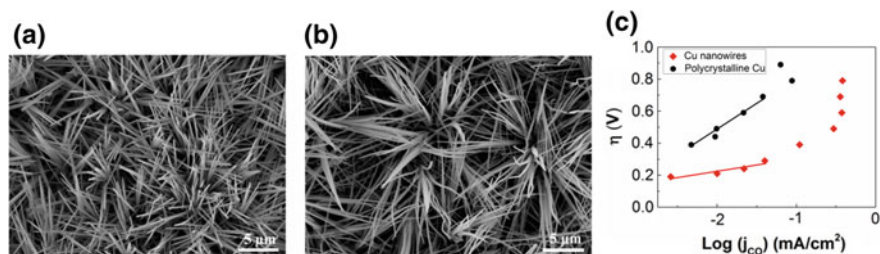


Fig. 11.11 SEM images of Cu(OH)₂ nanowires before (a) and after (b) annealing in air at 150 °C for 2 h, respectively. **c** Tafel plots of the CO partial current density for polycrystalline Cu and Cu nanowires. Reprinted with permission from Ref. [55]

conditions. The Tafel slope of ~ 110 mV/dec for Cu nanowire arrays shown in Fig. 11.11c indicates a fast initial electron transfer to CO₂ for the formation of adsorbed CO₂^{•-} intermediate. Thus, the improved catalytic selectivity for the reduction of CO₂ to CO is ascribed to the enhanced stabilization for the CO₂^{•-} intermediate on the high surface area Cu nanowire arrays.

It was also recently demonstrated that highly dense Cu nanowires for the electrochemical reduction of CO₂ [58]. CuO nanowires were prepared by the oxidation of Cu mesh in air and then reduced by annealing in the presence of hydrogen or applying a cathodic electrochemical potential to produce Cu nanowires. These nanowires showed the distinct catalytic selectivity for CO₂ reduction, which is linked to the different nanoscale crystalline and surface structures. The authors found that the Cu nanowires fabricated by the electrochemical reduction of CuO exhibited a FE toward CO as high as $\sim 60\%$ at overpotentials of less than 0.4 V [58].

At more negative potentials, hydrocarbon gas phase products on Cu nanowire arrays were observed [55]. Smith et al. tuned the selectivity of hydrocarbon products on Cu nanowire arrays by systematically varying the length and density of the Cu nanowires which can provide a high local pH within the nanowire arrays (Fig. 11.12) [59]. With increasing the Cu nanowire length ($\geq 2.4 \pm 0.56$ μm), the formation of n-propanol was detected along with CO, HCOOH and C₂H₄. On longer Cu nanowires ($\geq 7.3 \pm 1.3$ μm), C₂H₆ formation appeared, accompanying with the ethanol formation. The formation of C₂H₆ has never been reported in the electrocatalytic reduction of CO₂ on smooth Cu, [8, 9, 11] but was detected on nanostructured Cu catalysts as a minor product [14, 23, 24]. The authors proposed a reaction pathway towards C₂H₆ from the intermediate (CH₃CH₂O) in path (ii), as shown in Scheme 11.1 (a route to C₂H₆ had never been reported before this study). Furthermore, an increased selectivity for C₂H₄ was observed on Cu nanowire arrays with increasing the Cu nanowire length and density (Fig. 11.12a), which is due to the improved formation of C₂H₄ through a CO coupling mechanism caused by a high local pH within the Cu nanowire arrays.

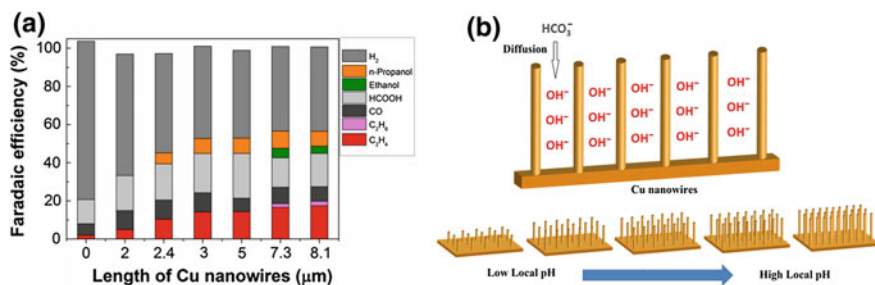
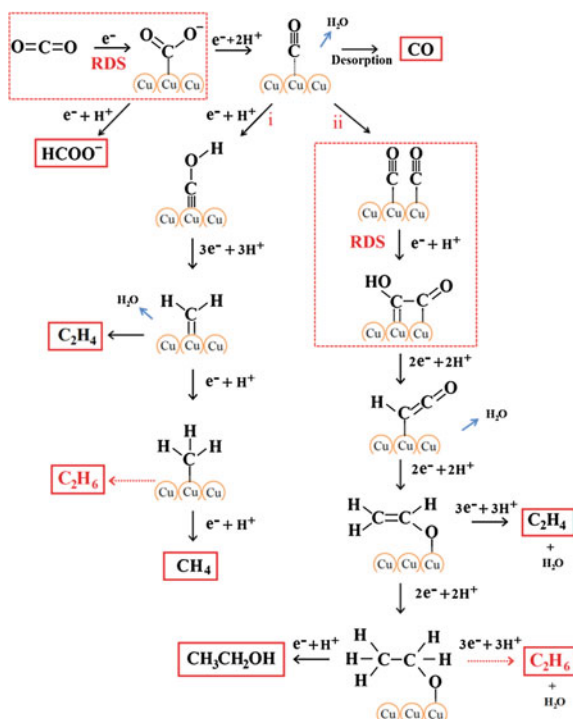


Fig. 11.12 **a** Faradaic efficiency for C₂H₄, C₂H₆, CO, HCOOH, ethanol, n-propanol and H₂ on Cu nanowire arrays with different lengths at -1.1 V versus RHE in CO₂-saturated 0.1 M KHCO₃ electrolytes (0 μm nanowire represents Cu foil). **b** Schematic illustration of the diffusion of electrolytes into Cu nanowire arrays. Reprinted with permission from Ref. [59]

Scheme 11.1 Proposed reaction paths for electrocatalytic reduction of CO₂ on Cu nanowire arrays, with path (i), *left*, showing COH formation, and path (ii), *right*, showing CO dimerization. In path (i), 2 CH₂ and 2 CH₃ intermediates are required for C₂H₄ and C₂H₆ formation, respectively. Reprinted with permission from Ref. [59]



11.3.3 Cu Nanofoam

Sen et al. investigated the electrochemical reduction of CO₂ over copper foams with hierarchical porosity [23]. Three-dimensional foams of copper were electrodeposited onto mechanically polished copper substrates. SEM images of copper foams

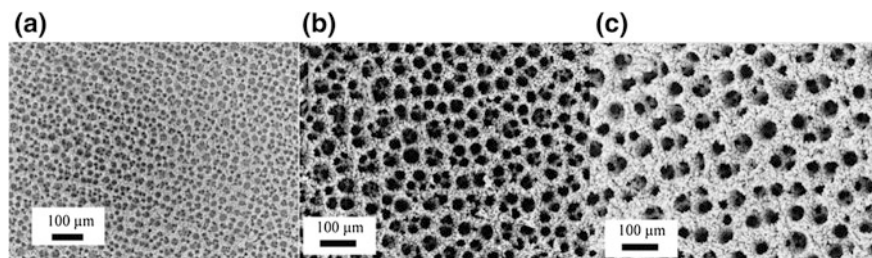


Fig. 11.13 SEM images of electrodeposited copper foams on a copper substrate for **a** 10 s; **b** 15 s; **c** 30 s. Reprinted with permission from Ref. [23]

prepared at different amounts of electrodeposition time are shown in Fig. 11.13. The electrocatalytic studies exhibited that the copper nanofoams are capable of reducing CO_2 to HCOOH , H_2 , and CO as major products along with small amounts of C_2H_4 , C_2H_6 , CH_4 , and C_3H_6 , which indicates a distinct product distribution (ethane and propylene were not observed on smooth copper) in comparison with that on smooth copper. The authors believed that these differences for the CO_2 reduction performance are attributed to high surface roughness, hierarchical porosity, and confinement of reactive species. In addition, it was observed that a gradual increase in the thickness the copper nanofoams with increasing electrodeposition time enhanced the FE of HCOOH formation by suppressing the electrochemical reduction of adsorbed H^+ to H_2 .

11.4 Oxide-Derived Metallic Nanocatalysts for CO_2 Reduction

While the reported metallic catalysts (Table 11.1) are competent for the electrocatalytic reduction of CO_2 , all have one or more following drawbacks: (1) high overpotential requirement for driving the CO_2 reduction. (2) poor catalytic selectivity, and (3) fast deactivation of electroreduction CO_2 process with favorable competing H_2 evolution. In order to improve the CO_2 reduction performance, an interesting way of preparing catalysts through the electrochemical reduction of metal oxides was recently proposed. In the process, the bulk metal is firstly oxidized, and then the metal oxide layer is directly utilized in the electrochemical CO_2 reduction in CO_2 -saturated electrolytes, reducing to metallic nanocatalysts during electrolysis. The recent development and progress of these oxide-derived (OD) catalysts are discussed in the following section.

11.4.1 Oxide-Derived Cu

Kanan et al. demonstrated the electrochemical reduction of CO₂ on a metallic Cu catalyst resulting from the reduction of thick Cu₂O films prepared by annealing Cu foil in air [14]. This sample formed by the electroreduction of a Cu₂O layer during the CO₂ reduction electrolysis was analyzed by XRD and XPS, indicating the complete reduction of the copper oxide layer. By systematically varying the original annealing temperature and time, it was found that annealing the Cu foil in air at 500 °C for 12 h results in a thick Cu₂O layer, which then forms a nanostructured Cu (OD-Cu) during electrocatalysis that are able to produce CO with ~40% FE and HCCOH with ~33% FE at -0.5 V versus RHE (Fig. 11.14a, b). Notably, the selectivity for CO (~40% FE) was maintained during the whole electrolysis of 7 h, revealing a dramatically improved catalytic stability for CO₂ reduction on OD-Cu. As shown in Fig. 11.14b, the OD-Cu exhibited a high FE for CO₂ reduction at much lower overpotential in comparison with the bulk Cu electrodes. The Tafel slope of ~116 mV/dec for OD-Cu in the low overpotential range (Fig. 11.14c) indicates the Cu formed by the electrochemical reduction of Cu₂O during electrolysis is in favor of the formation of CO₂^{•-} intermediate, resulting in the improved catalytic activity for CO₂ reduction.

Furthermore, Kas et al. investigated the electrocatalytic CO₂ reduction on copper nanoparticles derived from different orientation of electrodeposited Cu₂O ([110] [111][100]) [22]. The authors reported that the initial crystal orientation of Cu₂O had a minor effect on the catalytic selectivity for CO₂ reduction. However, it was found that the thickness of the initial Cu₂O layer strongly influenced the product selectivity, which is consistent with the previous study on OD-Cu [14].

The electrochemical reduction of CO₂ into fuels such as hydrocarbons on Cu catalysts is a complex multistep reaction with adsorbed intermediates, most notably adsorbed CO. Thus, CO reduction activity was investigated on OD-Cu, producing liquid products (ethanol, acetate and n-propanol) with nearly 50% FE at moderate potentials [53]. In order to correlate a particular structural feature of oxide-derived Cu with the catalytic activity, the authors proposed that the Cu catalysts

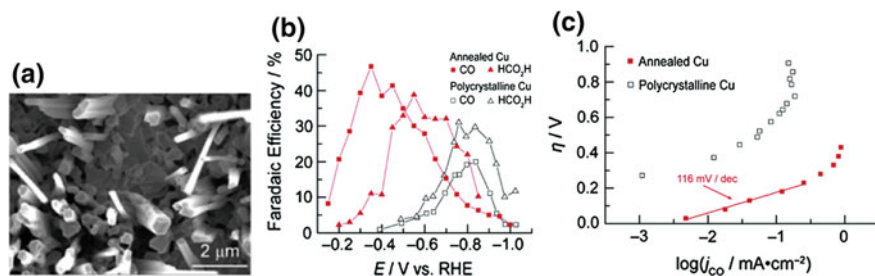


Fig. 11.14 a SEM image of OD-Cu. b Faradaic efficiencies for CO and HCOOH versus potential. And c CO partial current density Tafel plots for polycrystalline Cu and Cu annealed at 500 °C for 12 h. Reprinted with permission from Ref. [14]

electrochemically reduced from copper oxide may obtain a high density of grain boundary surfaces, likely resulting in a highly active sites for CO₂ reduction [53]. A temperature-programmed desorption (TPD) of CO was utilized to probe the surface chemistry of OD-Cu, revealing a high CO reduction activity on OD-Cu is linked to the active sites that bond CO more strongly in comparison with low-index and stepped Cu facets [60]. It was proposed that the strong binding sites with CO are supported by grain boundaries on the OD-Cu, which are only accessible in this nanostructured platform.

11.4.2 Oxide-Derived Au

It was reported that Au was the most efficient metal catalyst for CO₂ reduction, exhibiting the best catalytic selectivity and activity for the electrocatalytic reduction of CO₂ to CO among the identified bulk metals, as shown in Table 11.1. The Cu NP films prepared by the electrochemical reduction of thick Cu₂O layers exhibited a dramatically improved catalytic activity for the electroreduction of CO₂ to CO at lower overpotential with high resistance to deactivation, compared to Cu foils. Similar to this OD-Cu, OD-Au nanocatalysts were also studied for CO₂ reduction [13]. Initially, the Au oxide layers were prepared on Au foil electrodes by applying periodic square-wave pulsed potentials in 0.5 M H₂SO₄. After the pulsed anodization on Au, the Au oxide layers were synthesized on Au foils.

The Au oxide layers on Au foils were directly utilized for CO₂ reduction in CO₂-saturated electrolytes and were electrochemically reduced to metallic Au at the beginning of electrolysis (Fig. 11.15a shows the SEM images of the oxide-derived Au). The significant distinct CO₂ reduction activity for OD-Au and polycrystalline Au were observed at low overpotentials, as shown in Fig. 11.15b. At a low overpotential of 0.24 V, the FE for CO formation on the OD-Au was maintained at ~96% over the course of an 8 h electrolysis experiment. Furthermore, the Tafel slope of 114 mV/dec (Fig. 11.15c) on polycrystalline Au indicates the rate determining step is the initial electron transfer to form an adsorbed CO₂^{•-} intermediate

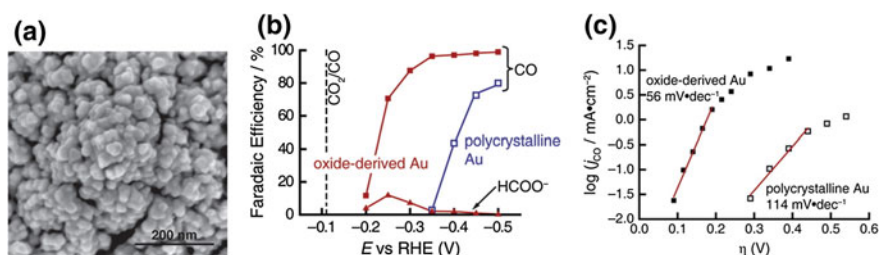
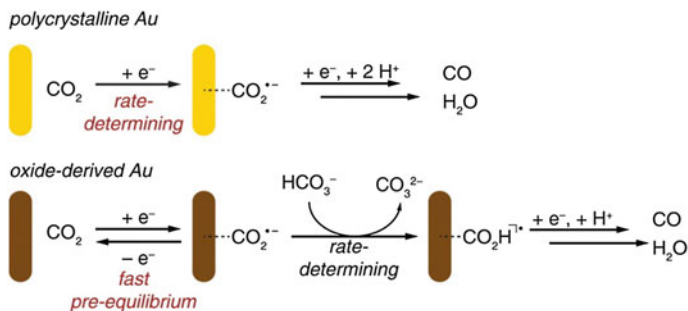


Fig. 11.15 **a** SEM image of oxide-derived Au NPs. **b** Faradaic efficiencies for CO and HCOOH, and **c** Tafel plots of CO partial current density of oxide-derived Au NPs and polycrystalline Au. Reprinted with permission from Ref. [13]



Scheme 11.2 Proposed mechanisms for CO₂ reduction to CO on polycrystalline Au and Oxide-Derived Au. Reprinted with permission from Ref. [13]

(Scheme 11.2). The poor stabilization of CO₂^{•-} intermediate is correlated with the high overpotential required on polycrystalline Au. In contrast, the active sites on OD-Au nanocatalysts offer the fast initial electron transfer (low Tafel slope in Fig. 11.15b), which results in the dramatically enhanced stabilization of CO₂^{•-} intermediate. The HCO₃⁻ concentration dependence studies on OD-Au showed an increase in the CO partial current density with gradually increasing the NaHCO₃ concentration, implying that the first proton donation from HCO₃⁻ is rate determining step on OD-Au (Scheme 11.2). Furthermore, a study on grain boundary effect showed that the catalytic activity for the electroreduction of CO₂ is linearly correlated with the grain boundary density on Au NPs and the high density of grain boundaries on OD-Au was thought to be linked to its enhanced catalytic performance [61].

11.4.3 Oxide-Derived Pb

Nanocrystalline Pb prepared by the electroreduction of PbO₂ exhibited a 700-fold lower H₂ selectivity compared to polycrystalline Pb, with maintaining the catalytic activity for CO₂ reduction [62]. OD-Pb showed a nearly 100% FE for HCOOH formation at the potential range from -1.0 to -0.75 V versus RHE in CO₂-saturated electrolytes, which is much better than the polycrystalline Pb (FF for HCOOH was 30% at -0.8 V vs. RHE). Notably, the high catalytic activity and selectivity for the electroreduction of CO₂ to HCOOH was more or less maintained during a prolonged electrolysis of 75 h. The dramatically improved CO₂ reduction performance on OD-Pb is attributed to its morphology and microstructure [62].

11.4.4 Oxide-Derived Ag

Recently, a porous-like nanostructured Ag catalyst (Fig. 11.16a, b) was prepared by electrochemically reducing Ag_2O which was synthesized by anodization of a Ag foil in alkaline solutions [63]. The results of the XRD patterns (Fig. 11.16c) and the Ag 3d XPS spectrum analysis (Fig. 11.16d) reveal that the electroreduction of Ag_2O to metallic Ag was complete within the detection limit of these characterization techniques. This OD-Ag exhibited an enhanced catalytic activity for the reduction of CO_2 , and the high selectivity for CO was shifted by >400 mV towards a lower overpotential than that of untreated polycrystalline Ag. Notably, the OD-Ag is able to reduce CO_2 to CO with $\sim 80\%$ EF at a moderate overpotential of 0.49 V, which is dramatically higher compared to that ($\sim 4\%$) of untreated polycrystalline Ag at identical conditions. The dramatically improved catalytic activity and

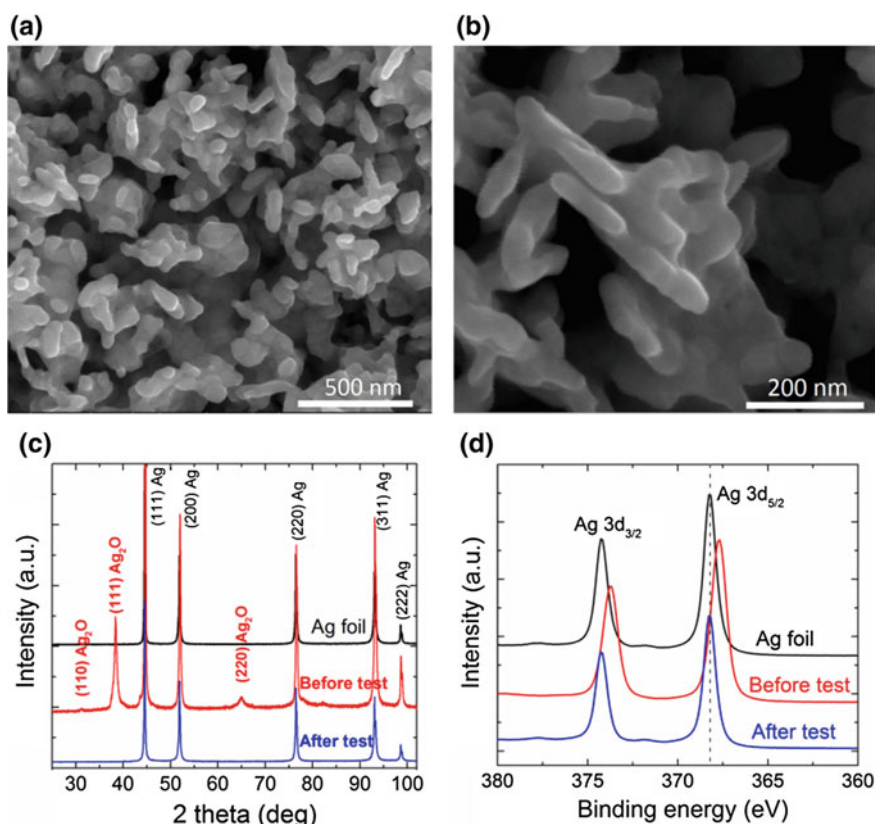


Fig. 11.16 **a** and **b** SEM images of oxide-derived Ag. **c** XRD patterns and **d** XPS spectrum of the polycrystalline Ag electrode (black line) and Ag oxide electrode before (red line) and after (blue line) CO_2 reduction electrolysis, respectively. Reprinted with permission from Ref. [63]

selectivity for CO₂ reduction to CO is likely correlated with of the nanostructured surfaces, resulting in highly active sites for stabilizing COOH⁻ intermediate. In addition, it was demonstrated that the porous-like nanostructured Ag catalyst is likely capable of generating a high local pH near the catalyst surface, which may also play a role in the improved CO₂ reduction along with suppressed H₂ evolution.

11.5 Bimetallic Nanocatalysts

Electrode surfaces provide the active sites for CO₂ reactions, and the reactants and other related species adsorbed on the electrode play an important role in the product selectivity of the CO₂ reduction. CO₂ can be electrochemically reduced to CO, HCOOH, and hydrocarbons on metal electrodes in aqueous solution. The intermediates formed on the electrode surface directly affect the product formed in the final steps of the catalytic reaction. Therefore, it is important to know the binding energy at the surface of different metals for different reaction intermediates.

Table 11.2 shows a comparison of the binding strength of CO₂ reduction intermediate species on FCC (111) single metal electrodes (adapted from Ref. [31]). The product distribution and selectivity of CO₂ reduction could be influenced by whether or not the related intermediates are adsorbed. Alloying an element that has high oxygen affinity into a catalyst may allow CHO to bind to the surface through the carbon and oxygen atoms, thus increasing the stability of CHO, which may affect the final product distribution and selectivity [30]. Thus, the interaction of the two different metallic atoms in the bimetallic alloy may significantly influence the catalytic activity and selectivity of alloy surface.

The electrocatalytic CO₂ reduction was performed on a nanostructured Cu-Au alloy prepared through electrochemical deposition with a nanoporous Cu film (NCF) as template, showing an improved catalytic selectivity for alcohols (methanol and ethanol) [64]. The authors found that the FE for alcohols was dependent on the nanostructured morphology and composition of Cu-Au alloys, as shown in Table 11.3. In addition, the FE of 15.9% for methanol was detected on Cu_{63.9}Au_{36.1}/NCF, which is ~19 times higher than that of pure Cu.

Yang et al. assembled monodisperse Au-Cu bimetallic NPs (Fig. 11.17a) with different compositions by implementing the solvent evaporation-mediated self-assembly approach and then the nanoparticle monolayer was transferred onto

Table 11.2 Comparison of the binding strength on FCC (111) transition metal facets. Reprinted with permission from Ref. [31]

Species on FCC(111) transition metal facets binding strength	
*CO	Rh > Pd > Ni > Pt > Cu > Au > Ag
*COH	Rh > Pt > Pd > Ni > Cu > Au > Ag
*CHO	Rh > Pt > Pd > Ni > Au > Cu > Ag
*OCH ₃	Ni > Rh > Cu > Ag > Pd > Pt > Au
*CH ₃	Pt > Rh > Ni > Pd > Cu > Au > Ag

Table 11.3 Faradaic efficiencies of main liquid products with different electrodes. Reprinted with permission from Ref. [64]

Electrode	Faradaic efficiency (%)	
	HCOOH	Alcohols (methanol and ethanol)
Bulk Cu	11.5	4.8
Nanostructured Cu	27.4	9.7
Cu _{63,9} Au _{36,1} /NCF	12.6	28
Cu _{70,6} Au _{29,4} /NCF	18.1	17.2
Cu _{81,3} Au _{19,7} /NCF	21.2	11.5

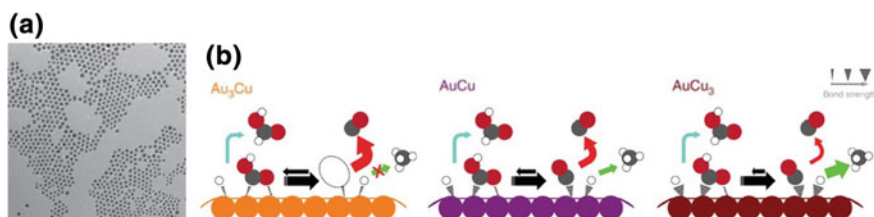


Fig. 11.17 **a** TEM image of AuCu₃ nanoparticles (scale bar, 100 nm). Average size 11.20 ± 1.65 nm. **b** Schematic showing the proposed mechanism for CO₂ reduction on the catalyst surface of Au-Cu bimetallic nanoparticles. Filled circles with grey is C, red is O and white is H. The relative intermediate binding strength is indicated by the stroke weight (on the top right corner). Additional binding between the COOH and the catalyst surface is presented as a dotted line. Arrows between the adsorbed COOH and adsorbed CO is to show the difference in probability of having COOH adsorbed on different types of surfaces. Coloured arrows indicate the pathway to each product: red for CO, blue for formate and green for hydrocarbons. Larger arrows indicate higher turnover. Reprinted with permission from Ref. [65]

a glassy carbon substrate for the electrochemical reduction of CO₂ [65]. With increasing the Cu content, different products were observed and the largest number in product distribution were found on pure Cu nanoparticles. The authors believed the degree of stabilization of the intermediates on these nanoparticle surfaces can be tuned by varying the composition of Au-Cu bimetallic NPs, which results in the different final products (Fig. 11.17b). Furthermore, the catalytic performance of these bimetallic catalysts was attributed to two factors: (1) the electronic effect on the binding strength of intermediates, which is linked to the change of electronic structure that is tuned with surface composition of the Au-Cu, and (2) the geometric effect that is correlated with the atomic arrangement at the active site that have a significant influence on the binding strength of intermediates [66].

The electrochemical CO₂ reduction was performed on a nanostructured Cu-In bimetallic alloy prepared by the in-situ electrochemical reduction of Cu₂O in InSO₄ electrolytes, and it was found that the In incorporation exhibited an enhanced selectivity for the electroreduction of CO₂ to CO with high catalytic stability [67]. At potential from -0.3 to -0.7 V versus RHE, CO was generated on Cu-In alloy catalysts as almost the only products in CO₂ reduction, and notably a FE of $\sim 90\%$

for CO formation was achieved on the alloy catalysts at -0.5 V versus RHE. A DFT study suggested that the incorporation of In may cause both local electronic effect and local geometric effect. The presence of In atoms has a significant effect on the binding energy of the associated intermediates adsorbed on Cu. Furthermore, the dramatically enhanced FE for the conversion of CO₂ into CO is also achieved on nanostructured Cu-Sn bimetallic electrocatalysts at decreased overpotentials [68].

Recently, a mesoporous nanostructured Pd-Cu bimetallic electrocatalyst was fabricated by an electrodeposition method for CO₂ reduction and Pd₇-Cu₃ exhibited a FE of more than 80% for selective CO formation at -0.8 V versus RHE [69]. The mesoporous nanostructure has a roughened surface, which could offer more active sites for the selective reduction of CO₂ to CO. In addition, first principle calculations suggested that Pd atoms on the surface of the bimetallic catalysts act as reactive centers with an increased adsorption ability of CO₂ and COOH, and the presence of Cu could modify the CO desorption ability. The authors believed that the catalytic activity is ascribed to the change of electronic structure of their neighboring element and adjustment of atomic arrangement in the active sites.

Koper et al. have used bimetallic Pd-Pt nanoparticles for the electrocatalytic CO₂ reduction [70]. They found that Pd-Pt nanoparticles had a low onset potential for the reduction of CO₂ to HCOOH, starting at 0 V versus RHE for HCOOH formation, which is close to the theoretical equilibrium potential of producing HCOOH (Eq. 11.2). In addition, the FE for HCOOH formation was dependent on the composition of the NPs and a high FE of 88% towards HCOOH formation was reached on Pd₇₀-Pt₃₀ at an applied potential of -0.4 V versus RHE.

While the progress on bimetallic catalysts for the electrochemical CO₂ reduction performance has been made, the fundamental understanding of the relationship between the bimetallic catalyst and catalytic activity of CO₂ reduction is still not very clear. The further understanding of the correlation of bimetallic catalyst with catalytic activity of CO₂ reduction is critical for reasonable designing the high-performance bimetallic catalysts.

11.6 Nano Carbon Catalysts

Carbon is a remarkable element, which can exist in a variety of stable forms such as diamond (or diamond-like amorphous film), [71] graphite, fullerenes (C₆₀) and carbon nanotubes (CNTs), [72] as shown in Fig. 11.18. Nanostructured carbon materials (such as graphene and CNTs) have attracted a great deal of interest in the past because of their unique structure and interesting electronic, physical and chemical properties [73]. Recently, nanostructured carbon materials including graphene, nano-diamond, carbon nanofibers (CNFs) and CNTs have been applied as the electrodes in the electrocatalytic CO₂ reduction due to the high catalytic selectivity, low cost and high stability.

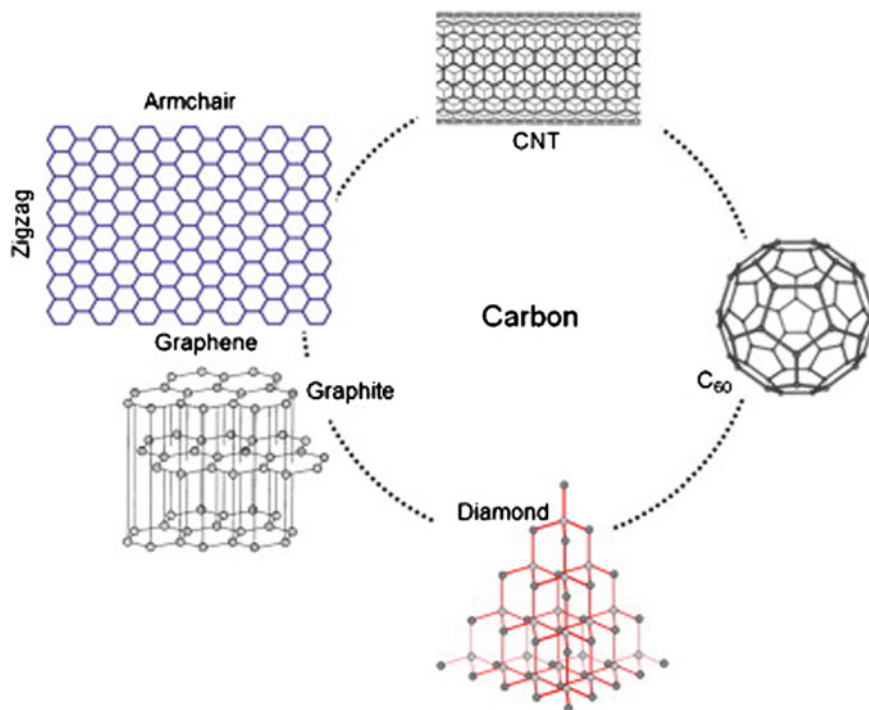


Fig. 11.18 Polymorphs of carbon. Reprinted with permission from Ref. [73]

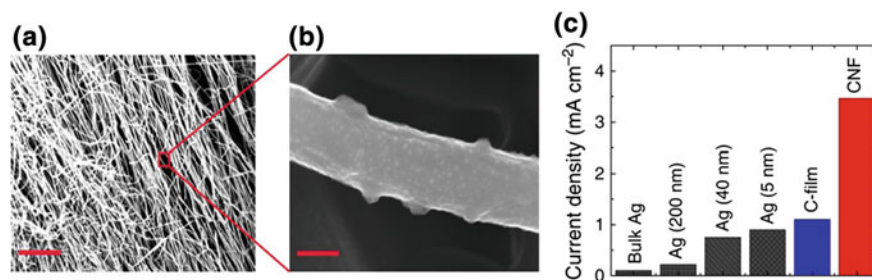


Fig. 11.19 **a** SEM image of the CNF mat displaying entangled fibers (scale bar, 5 mm), **b** high-resolution SEM image on individual fibers (scale bar, 200 nm). **c** Current density for CO₂ reduction at different (bulk Ag, Ag nanoparticles and CNF) electrodes in pure EMIM-BF₄ electrolyte. Reprinted with permission from Ref. [74]

Kumar et al. reported the electrocatalytic CO₂ reduction on metal-free carbon nanofibers prepared by pyrolysis of electrospun nanofibre mats of heteroatomic polyacrylonitrile (PAN) polymer (Fig. 11.19) [74]. It was confirmed that the presence of nitrogen atoms (defects) in CNFs due to the existence of nitrogen atoms in the backbone of the precursor (PAN). The catalytic activity of CO₂ reduction was

performed in CO₂-saturated 1-ethyl-3-methylimidazolium tetrafluoroborate (EMIM-BF₄) electrolyte due to its high CO₂ solubility. The CNFs catalyst showed a very small overpotential of 0.17 V for driving CO₂ reduction to CO (the CO₂/CO equilibrium potential is -0.11 V vs. RHE) and more than an order of magnitude higher current density in comparison with the bulk silver catalyst under similar experimental conditions (Fig. 11.19). Furthermore, a FE of 98% for CO formation was detected at the potential of -0.57 V versus SHE. The high CO₂ reduction performance of CNFs is attributed to its nanofibrillar morphology and rough surface (due to the fractal-like corrugations on the surface) which offers high number of active catalytic sites and high binding energies of key intermediates on the CNF surface.

Nitrogen-doped carbon nanotubes (NCNTs) followed with the adsorption of Polyethylenimine (PEI) functions as a co-catalyst were synthesized by ammonia plasma treatment of CNTs on glassy carbon substrates for CO₂ reduction [75]. The combination of N-doping of CNTs and PEI exhibited a significant reduction for overpotential and improved catalytic performance for the selective reduction of CO₂ to HCOOH with a high FE (87%) and current density (9.5 mA/cm²) in CO₂-saturated 0.1 KHCO₃ aqueous solutions. The rate determining step for CO₂ reduction is the initial electron transfer to CO₂ for the CO₂^{•-} intermediate and CO₂ is adsorbed to the basic nitrogen binding sites in NCNT for reducing to CO₂^{•-} in the proposed mechanism. The PEI works as a co-catalyst to improve the stabilization of CO₂^{•-} intermediate by a H-bond interaction, NCNT-N-C(O)O⁻ ··· H-N-PEI. Thus, the PEI overlayer and N-doping could provide a synergistic effect, creating a local environment for stabilizing CO₂^{•-} intermediate from CO₂ with significantly reduced overpotential.

N incorporated CNT arrays with a total N content of 5 atom% were fabricated by liquid chemical vapor deposition (CVD) method for CO₂ reduction, acting as a highly selective, efficient and stable electrocatalyst for the catalytic reduction of CO₂ to CO (Fig. 11.20) [76]. The high selectivity toward the production of CO was achieved on NCNTs (The FE of ~80% for CO formation), as shown in Fig. 11.20b. In contrast, pristine CNTs show much high overpotential for CO₂ reduction with low catalytic activity and selectivity for the electroreduction of CO₂ to CO (Fig. 11.20). The improved catalytic activity for CO₂ reduction on NCNTs is attributed high electrical conductivity, pyridinic N defects (preferable catalytic sites), low free energy for CO₂ activation and high barrier for hydrogen evolution. In addition, the reaction mechanism of electroreduction of CO₂ to CO on the pristine CNT and NCNT surfaces through the adsorbed intermediates was studied by DFT calculations, suggesting that the suitable binding energy of the key intermediates enables strong adsorption of COOH and feasible CO desorption that contributes to the high selectivity toward CO formation (Fig. 11.21).

N-doped three-dimensional (3D) graphene foam (NG) fabricated by CVD has been used as a electrocatalyst for the electrocatalytic CO₂ reduction [77]. The various N-defect structures and content incorporated graphene foams were synthesized by a post growth doping process performed at various temperatures for CO₂ reduction (Fig. 11.22). N-doped NG processed at 800 °C (denoted as NG-800)

exhibited that the selective reduction of CO_2 to CO started to be observed at -0.30 V versus RHE with a FE of 25%, which corresponds to an overpotential of 0.19 V for CO production. In addition, the maximum FE for CO production on NG-800 was reached to be $\sim 85\%$ with high stability during the electrolysis of 5 h at -0.58 V versus RHE, corresponding to an overpotential of 0.47 V. The correlation between catalytic activity and the N-defects along with its corresponding potential versus concentrations of different N species (Fig. 11.22c) shows that the maximum FE for CO formation increases and the corresponding potential shifts anodically with increasing the pyridinic-N content. These results suggested pyridinic-N is the most active site for CO_2 reduction. The high catalytic selectivity for CO and low overpotential on the NG-800 could be linked to the high pyridinic-N concentration which acts as the active site for CO_2 reduction.

N-doped nanodiamond coated on Si rod array has been demonstrated as an efficient and stable nonmetallic catalyst for the electrocatalytic CO_2 reduction in CO_2 -saturated 0.5 NaHCO_3 electrolytes [78]. The onset potential for CO_2 reduction was found to be -0.36 V versus RHE. The FE for acetate (CH_3COOH) formation

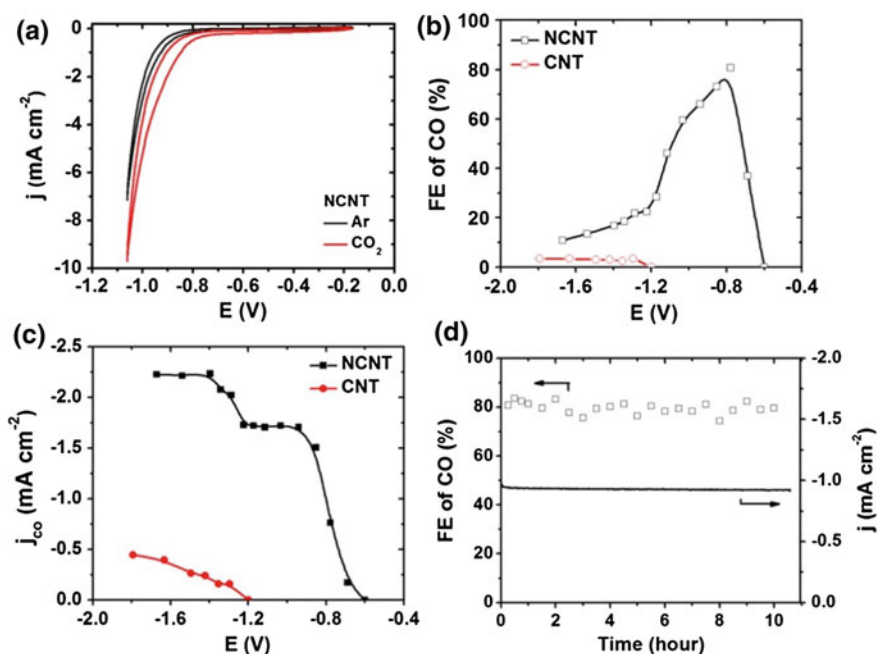


Fig. 11.20 Performance of NCNTs for electrochemical reduction of CO_2 . **a** CVs for NCNTs in Ar- and CO_2 -saturated 0.1 M KHCO_3 electrolyte, 50 mVs^{-1} . **b** Dependence of FE of CO on applied cell potential during electrocatalysis of CO_2 reduction for both NCNTs and CNTs catalysts. **c** Partial current density of CO versus applied cell potential for NCNTs and CNTs catalysts. **d** Stability of performance of NCNTs for CO_2 reduction operated at potentiostatic mode of -0.8 V for 10 h. Both current density and FE of CO remain steady over the duration of the test. Reprinted with permission from Ref. [76]

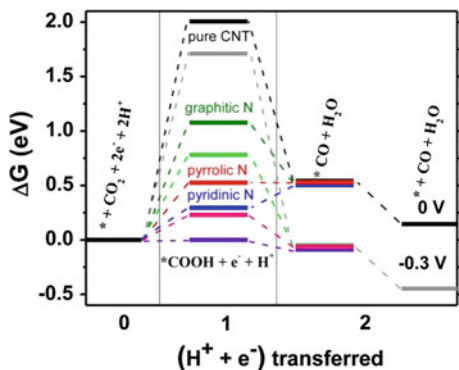


Fig. 11.21 Calculated free energy diagram for CO₂ electroreduction to CO on pristine CNTs and NCNTs. Reprinted with permission from Ref. [76]

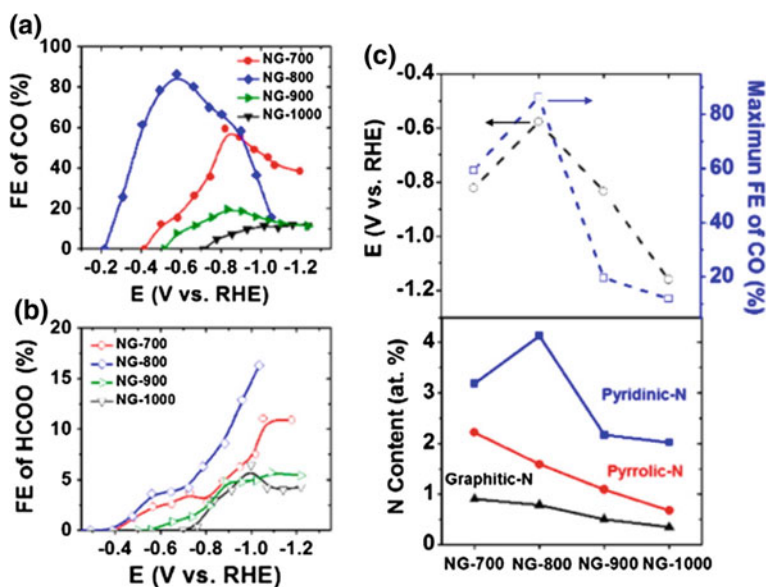


Fig. 11.22 Comparison of the electrocatalytic activities of nitrogen-doped graphene with doping temperature ranging from 700 to 1000 °C. **a** Faradaic efficiency of CO versus potential. **b** Faradaic efficiency of HCOO⁻ versus potential. **c** Maximum faradaic efficiency of CO and its corresponding potential versus N functionality content. Reprinted with permission from Ref. [77]

(77.3–77.6%) was detected along with HCOOH (13.6–14.6%) at the applied potentials from -0.55 to -1.3 V versus RHE. It was found that the total FE of CH₃COOH and HCOOH reached 91.8% at -1.0 V versus RHE. The improved CO₂ reduction activity was ascribed to N-doped sp³ carbon which was highly active for the electrocatalytic CO₂ reduction.

11.7 Summary and Outlook

This chapter provides a review of the development and recent trends on nanostructured catalysts for the electrocatalytic reduction of CO₂. Nanostructured Au, Ag, Zn, Pd, Cu, bimetallic and oxide-derived metal catalysts, and the recent discoveries in the application of metal-free nanostructured carbon for the electroreduction of CO₂ were reviewed.

According to the results discussed in this chapter, nanostructured catalysts are capable of electrochemically reducing CO₂ with high selectivity and efficiency. It is generally accepted that nanostructured metal catalysts could offer an abundance of edge sites which are active for certain intermediate formation (e.g. COOH[•]), resulting in the enhanced catalytic CO₂ reduction performance. In other words, the nanostructured catalysts could offer low-coordinated surface sites, which may facilitate the key intermediates formation by reducing the activation barrier of CO₂ reduction. Furthermore, the large surface area (roughened surface) provided by nanostructured catalysts is capable of adapting contamination and enhancing tolerance to heavy metal impurities, resulting in a better catalytic stability performance in CO₂ reduction on nanostructured catalysts in comparison with bulk catalysts.

The interaction of the two different metallic atoms in the bimetallic alloys may significantly influence the catalytic activity for the electrocatalytic CO₂ reduction. The changed catalytic activity on these bimetallic catalysts could be attributed to: (1) the electronic effect on the binding strength of intermediates, which is due to that electronic structure may be tuned by surface composition of two different metallic elements, (2) the geometric effect that is linked to the atomic arrangement that plays a significant role in the binding strength of intermediates. Thereby, it is critical to rationally design a bimetallic catalysts that could facilitate certain intermediate formation, leading to selective CO₂ reduction.

Nanostructured carbon could be a promising candidate as a metal-free electrocatalyst due to its low cost and high stability and catalytic activity for CO₂ reduction. N defects (or N doping) were generally presented in nanostructured carbon catalysts with the significantly enhanced catalytic activity and selectivity because N species were suggested to be the active site for CO₂ reduction. However, pristine nanostructured carbon catalysts have poor catalytic activity for CO₂ reduction. Different element doping could be designed to improve the catalytic activity on nanostructured carbon catalysts. We believe that the nanostructured carbon catalysts are also highly important for CO₂ reduction due to their high stability, low cost, earth abundance and comparable catalytic performance with expensive noble metal catalysts.

References

1. Davis, S.J., K. Caldeira, and H.D. Matthews. 2010. Future CO₂ emissions and climate change from existing energy infrastructure. *Science* 329: 1330–1333. doi:10.1126/science.1188566.
2. Hoegh-Guldberg, O., P.J. Mumby, A.J. Hooten, R.S. Steneck, P. Greenfield, E. Gomez, C.D. Harvell, P.F. Sale, A.J. Edwards, K. Caldeira, N. Knowlton, C.M. Eakin, R. Iglesias-Prieto, N. Muthiga, R.H. Bradbury, A. Dubi, and M.E. Hatzioiols. 2007. Coral reefs under rapid climate change and ocean acidification. *Science* 318: 1737–1742. doi:10.1126/science.1152509.
3. Orr, J.C., V.J. Fabry, O. Aumont, L. Bopp, S.C. Doney, R.A. Feely, A. Gnanadesikan, N. Gruber, A. Ishida, F. Joos, R.M. Key, K. Lindsay, E. Maier-Reimer, R. Matear, P. Monfray, A. Mouchet, R.G. Najjar, G.-K. Plattner, K.B. Rodgers, C.L. Sabine, J.L. Sarmiento, R. Schlitzer, R.D. Slater, I.J. Totterdell, M.-F. Weirig, Y. Yamanaka, and A. Yool. 2005. Anthropogenic ocean acidification over the twenty-first century and its impact on calcifying organisms. *Nature* 437: 681–686. doi:10.1038/nature04095.
4. Hall-Spencer, J.M., R. Rodolfo-Metalpa, S. Martin, E. Ransome, M. Fine, S.M. Turner, S. J. Rowley, D. Tedesco, and M.-C. Buia. 2008. Volcanic carbon dioxide vents show ecosystem effects of ocean acidification. *Nature* 454: 96–99. doi:10.1038/nature07051.
5. Lu, Q., J. Rosen, Y. Zhou, G.S. Hutchings, Y.C. Kimmel, J.G. Chen, and F. Jiao. 2014. A selective and efficient electrocatalyst for carbon dioxide reduction. *Nature Communications* 5: 3242. doi:10.1038/ncomms4242.
6. Whipple, D.T., and P.J.A. Kenis. 2010. Prospects of CO₂ utilization via direct heterogeneous electrochemical reduction. *The Journal of Physical Chemistry Letters* 1: 3451–3458. doi:10.1021/jz1012627.
7. DiMeglio, J.L., and J. Rosenthal. 2013. Selective conversion of CO₂ to CO with high efficiency using an inexpensive bismuth-based electrocatalyst. *Journal of the American Chemical Society* 135: 8798–8801. doi:10.1021/ja4033549.
8. Hori, Y. 2008. Modern aspects of electrochemistry. In *Electrochemical CO₂ Reduction on Metal Electrodes*, vol. 42, ed. Vayenas, E.C.G., R.E. White, and M.E. Gamboa-Aldeco, 89. New York: Springer. doi:10.1007/978-0-387-49489-0_3.
9. Kuhl, K.P., E.R. Cave, D.N. Abram, and T.F. Jaramillo. 2012. New insights into the electrochemical reduction of carbon dioxide on metallic copper surfaces. *Energy & Environmental Science* 5: 7050–7059. doi:10.1039/c2ee21234j.
10. Qiao, J., Y. Liu, F. Hong, and J. Zhang. 2014. A review of catalysts for the electroreduction of carbon dioxide to produce low-carbon fuels. *Chemical Society Reviews* 43: 631–675. doi:10.1039/c3cs60323g.
11. Gattrell, M., N. Gupta, and A. Co. 2006. A review of the aqueous electrochemical reduction of CO₂ to hydrocarbons at copper. *Journal of Electroanalytical Chemistry* 594: 1–19. doi:10.1016/j.jelechem.2006.05.013.
12. Chen, Y., and M.W. Kanan. 2012. Tin oxide dependence of the CO₂ reduction efficiency on tin electrodes and enhanced activity for tin/tin oxide thin-film catalysts. *Journal of the American Chemical Society* 134: 1986–1989. doi:10.1021/ja2108799.
13. Chen, Y., C.W. Li, and M.W. Kanan. 2012. Aqueous CO₂ reduction at very low overpotential on oxide-derived Au nanoparticles. *Journal of the American Chemical Society* 134: 19969–19972. doi:10.1021/ja309317u.
14. Li, C.W., and M.W. Kanan. 2012. CO₂ reduction at low overpotential on Cu electrodes resulting from the reduction of thick Cu₂O films. *Journal of the American Chemical Society* 134: 7231–7234. doi:10.1021/ja3010978.
15. Hori, Y., K. Kikuchi, and S. Suzuki. 1985. Production of CO and CH₄ in electrochemical reduction of CO₂ at metal electrodes in aqueous hydrogencarbonate solution. *Chemistry Letters* 1695–1698. doi:10.1246/cl.1985.1695.

16. Hori, Y., H. Wakebe, T. Tsukamoto, and O. Koga. 1994. Electrocatalytic process of CO selectivity in electrochemical reduction of CO₂ at metal electrodes in aqueous media. *Electrochimica Acta* 39: 1833–1839. doi:10.1016/0013-4686(94)85172-7.
17. Hoshi, N., M. Kato, and Y. Hori. 1997. Electrochemical reduction of CO₂ on single crystal electrodes of silver Ag(111), Ag(100) and Ag(110). *Journal of Electroanalytical Chemistry* 440: 283–286. doi:10.1016/S0022-0728(97)00447-6.
18. Hori, Y., I. Takahashi, O. Koga, and N. Hoshi. 2002. Selective formation of C2 compounds from electrochemical reduction of CO₂ at a series of copper single crystal electrodes. *The Journal of Physical Chemistry B* 106: 15–17. doi:10.1021/jp013478d.
19. Xiao, J., A. Kuc, T. Frauenheim, and T. Heine. 2014. CO₂ reduction at low overpotential on Cu electrodes in the presence of impurities at the subsurface. *Journal of Materials Chemistry A* 2: 4885. doi:10.1039/c3ta14755j.
20. Hatsukade, T., K.P. Kuhl, E.R. Cave, D.N. Abram, and T.F. Jaramillo. 2014. Insights into the electrocatalytic reduction of CO₂ on metallic silver surfaces. *Physical Chemistry Chemical Physics: PCCP* 16: 13814–13819. doi:10.1039/C4CP00692E.
21. Reske, R., H. Mistry, F. Behafarid, B. Roldan Cuenya, and P. Strasser. 2014. Particle size effects in the catalytic electroreduction of CO₂ on Cu nanoparticles. *Journal of the American Chemical Society* 136: 6978–6986. doi:10.1021/ja500328k.
22. Kas, R., R. Kortlever, A. Milbrat, M.T.M. Koper, G. Mul, and J. Baltrusaitis. 2014. Electrochemical CO₂ reduction on Cu₂O-derived copper nanoparticles: Controlling the catalytic selectivity of hydrocarbons. *Physical Chemistry Chemical Physics: PCCP* 16: 12194. doi:10.1039/c4cp01520g.
23. Sen, S., D. Liu, and G.T.R. Palmore. 2014. Electrochemical reduction of CO₂ at copper nanofoams. *ACS Catalysis* 4: 3091–3095. doi:10.1021/cs500522g.
24. Tang, W., A.A. Peterson, A.S. Varela, Z.P. Jovanov, L. Bech, W.J. Durand, S. Dahl, J.K. Nørskov, and I. Chorkendorff. 2012. The importance of surface morphology in controlling the selectivity of polycrystalline copper for CO₂ electroreduction. *Physical Chemistry Chemical Physics* 14: 76–81. doi:10.1039/c1cp22700a.
25. Hansen, H.A., J.B. Varley, A.A. Peterson, and J.K. Nørskov. 2013. Understanding trends in the electrocatalytic activity of metals and enzymes for CO₂ reduction to CO. *The Journal of Physical Chemistry Letters* 4: 388–392. doi:10.1021/jz3021155.
26. Y. Hori, K. Kikuchi, A. Murata, and S. Suzuki. 1986. Production of methane and ethylene in electrochemical reduction of carbon dioxide at copper electrode in aqueous hydrogencarbonate solution. *Chemistry Letters* 897–898. doi:10.1246/cl.1986.897.
27. Li, Y., S.H. Chan, and Q. Sun. 2015. Heterogeneous catalytic conversion of CO₂: A comprehensive theoretical review. *Nanoscale* 7: 8663–8683. doi:10.1039/c5nr00092k.
28. Kortlever, R., J. Shen, K.J.P. Schouten, F. Calle-Vallejo, and M.T.M. Koper. 2015. Catalysts and reaction pathways for the electrochemical reduction of carbon dioxide. *The Journal of Physical Chemistry Letters* 6: 4073–4082. doi:10.1021/acs.jpcllett.5b01559.
29. Peterson, A.A., F. Abild-Pedersen, F. Studt, J. Rossmeisl, and J.K. Nørskov. 2010. How copper catalyzes the electroreduction of carbon dioxide into hydrocarbon fuels. *Energy & Environmental Science* 3: 1311. doi:10.1039/c0ee00071j.
30. Peterson, A.A., and J.K. Nørskov. 2012. Activity descriptors for CO₂ electroreduction to methane on transition-metal catalysts. *The Journal of Physical Chemistry Letters* 3: 251–258. doi:10.1021/jz201461p.
31. Shi, C., H.A. Hansen, A.C. Lausche, and J.K. Nørskov. 2014. Trends in electrochemical CO₂ reduction activity for open and close-packed metal surfaces. *Physical Chemistry Chemical Physics* 16: 4720. doi:10.1039/c3cp54822h.
32. Kuhl, K.P., T. Hatsukade, E.R. Cave, D.N. Abram, J. Kibsgaard, and T.F. Jaramillo. 2014. Electrocatalytic conversion of carbon dioxide to methane and methanol on transition metal surfaces. *Journal of the American Chemical Society* 136: 14107–14113. doi:10.1021/ja505791r.
33. Mohamed, R.M., D.L. McKinney, and W.M. Sigmund. 2012. Enhanced nanocatalysts. *Materials Science and Engineering: R: Reports* 73: 1–13. doi:10.1016/j.mser.2011.09.001.

34. Lu, Q., J. Rosen, and F. Jiao. 2015. Nanostructured metallic electrocatalysts for carbon dioxide reduction. *ChemCatChem* 7: 38–47. doi:[10.1002/cctc.201402669](https://doi.org/10.1002/cctc.201402669).
35. Rosen, J., G.S. Hutchings, Q. Lu, S. Rivera, Y. Zhou, D.G. Vlachos, and F. Jiao. 2015. Mechanistic insights into the electrochemical reduction of CO₂ to CO on nanostructured Ag surfaces. *ACS Catalysis* 5: 4293–4299. doi:[10.1021/acscatal.5b00840](https://doi.org/10.1021/acscatal.5b00840).
36. Nursanto, E.B., H.S. Jeon, C. Kim, M.S. Jee, J.H. Koh, Y.J. Hwang, and B.K. Min. 2016. Gold catalyst reactivity for CO₂ electro-reduction: From nano particle to layer. *Catalysis Today* 260: 107–111. doi:[10.1016/j.cattod.2015.05.017](https://doi.org/10.1016/j.cattod.2015.05.017).
37. Lee, H.-E., K.D. Yang, S.M. Yoon, H.-Y. Ahn, Y.Y. Lee, H. Chang, D.H. Jeong, Y.-S. Lee, M.Y. Kim, and K.T. Nam. 2015. Concave rhombic dodecahedral Au nanocatalyst with multiple high-index facets for CO₂ reduction. *ACS Nano* 9: 8384–8393. doi:[10.1021/acsnano.5b03065](https://doi.org/10.1021/acsnano.5b03065).
38. Kauffman, D.R., D. Alfonso, C. Matranga, H. Qian, and R. Jin. 2012. Experimental and computational investigation of Au₂₅ clusters and CO₂: A unique interaction and enhanced electrocatalytic activity. *Journal of the American Chemical Society* 134: 10237–10243. doi:[10.1021/ja303259q](https://doi.org/10.1021/ja303259q).
39. Zhu, W., R. Michalsky, Ö. Metin, H. Lv, S. Guo, C.J. Wright, X. Sun, A.A. Peterson, and S. Sun. 2013. Monodisperse Au nanoparticles for selective electrocatalytic reduction of CO₂ to CO. *Journal of the American Chemical Society* 135: 16833–16836. doi:[10.1021/ja409445p](https://doi.org/10.1021/ja409445p).
40. Zhu, W., Y.-J. Zhang, H. Zhang, H. Lv, Q. Li, R. Michalsky, A.A. Peterson, and S. Sun. 2014. Active and selective conversion of CO₂ to CO on ultrathin Au nanowires. *Journal of the American Chemical Society* 136: 16132–16135. doi:[10.1021/ja5095099](https://doi.org/10.1021/ja5095099).
41. Kim, C., H.S. Jeon, T. Eom, M.S. Jee, H. Kim, C.M. Friend, B.K. Min, and Y.J. Hwang. 2015. Achieving selective and efficient electrocatalytic activity for CO₂ reduction using immobilized silver nanoparticles. *Journal of the American Chemical Society* 137: 13844–13850. doi:[10.1021/jacs.5b06568](https://doi.org/10.1021/jacs.5b06568).
42. Salehi-Khojin, A., H.M. Jhong, B.A. Rosen, W. Zhu, S. Ma, P.J.A. Kenis, and R.I. Masel. 2013. Nanoparticle silver catalysts that show enhanced activity for carbon dioxide electrolysis. *Journal of Physical Chemistry C* 117: 1627–1632. doi:[10.1021/jp310509z](https://doi.org/10.1021/jp310509z).
43. Rosen, J., G.S. Hutchings, Q. Lu, R.V. Forest, A. Moore, and F. Jiao. 2015. Electrodeposited Zn dendrites with enhanced CO selectivity for electrocatalytic CO₂ reduction. *ACS Catalysis* 5: 4586–4591. doi:[10.1021/acscatal.5b00922](https://doi.org/10.1021/acscatal.5b00922).
44. Gao, D., H. Zhou, J. Wang, S. Miao, F. Yang, G. Wang, J. Wang, and X. Bao. 2015. Size-dependent electrocatalytic reduction of CO₂ over Pd nanoparticles. *Journal of the American Chemical Society* 137: 4288–4291. doi:[10.1021/jacs.5b00046](https://doi.org/10.1021/jacs.5b00046).
45. Hinogami, R., S. Yotsuhashi, M. Deguchi, Y. Zenitani, H. Hashiba, and Y. Yamada. 2012. Electrochemical reduction of carbon dioxide using a copper rubeanate metal organic framework. *ECS Electrochemistry Letters* 1: H17–H19. doi:[10.1149/2.001204eel](https://doi.org/10.1149/2.001204eel).
46. Kornienko, N., Y. Zhao, C.S. Kley, C. Zhu, D. Kim, S. Lin, C.J. Chang, O.M. Yaghi, and P. Yang. 2015. Metal-organic frameworks for electrocatalytic reduction of carbon dioxide. *Journal of the American Chemical Society* 137: 14129–14135. doi:[10.1021/jacs.5b08212](https://doi.org/10.1021/jacs.5b08212).
47. Hod, I., M.D. Sampson, P. Deria, C.P. Kubiak, O.K. Farha, and J.T. Hupp. 2015. Fe-porphyrin-based metal-organic framework films as high-surface concentration, heterogeneous catalysts for electrochemical reduction of CO₂. *ACS Catalysis* 5: 6302–6309. doi:[10.1021/acscatal.5b01767](https://doi.org/10.1021/acscatal.5b01767).
48. Hori, Y., H. Wakebe, T. Tsukamoto, and O. Koga. 1995. Adsorption of CO accompanied with simultaneous charge transfer on copper single crystal electrodes related with electrochemical reduction of CO₂ to hydrocarbons. *Surface Science* 335: 258–263. doi:[10.1016/0039-6028\(95\)00441-6](https://doi.org/10.1016/0039-6028(95)00441-6).
49. Schouten, K.J.P., Z. Qin, E.P. Gallent, and M.T.M. Koper. 2012. Two pathways for the formation of ethylene in CO reduction on single-crystal copper electrodes. *Journal of the American Chemical Society* 134: 9864–9867. doi:[10.1021/ja302668n](https://doi.org/10.1021/ja302668n).

50. Hori, Y., R. Takahashi, Y. Yoshinami, and A. Murata. 1997. Electrochemical reduction of CO at a copper electrode. *The Journal of Physical Chemistry B* 101: 7075–7081. doi:[10.1021/jp970284i](https://doi.org/10.1021/jp970284i).
51. Schouten, K.J.P., Y. Kwon, C.J.M. van der Ham, Z. Qin, and M.T.M. Koper. 2011. A new mechanism for the selectivity to C1 and C2 species in the electrochemical reduction of carbon dioxide on copper electrodes. *Chemical Science* 2: 1902. doi:[10.1039/c1sc00277e](https://doi.org/10.1039/c1sc00277e).
52. Hori, Y., I. Takahashi, O. Koga, and N. Hoshi. 2003. Electrochemical reduction of carbon dioxide at various series of copper single crystal electrodes. *Journal of Molecular Catalysis A: Chemical* 199: 39–47. doi:[10.1016/S1381-1169\(03\)00016-5](https://doi.org/10.1016/S1381-1169(03)00016-5).
53. Li, C.W., J. Ciston, and M.W. Kanan. 2014. Electroreduction of carbon monoxide to liquid fuel on oxide-derived nanocrystalline copper. *Nature* 508: 504–507. doi:[10.1038/nature13249](https://doi.org/10.1038/nature13249).
54. Manthiram, K., B.J. Beberwyck, and A.P. Alivisatos. 2014. Enhanced electrochemical methanation of carbon dioxide with a dispersible nanoscale copper catalyst. *Journal of the American Chemical Society* 136: 13319–13325. doi:[10.1021/ja5065284](https://doi.org/10.1021/ja5065284).
55. Ma, M., K. Djanashvili, and W.A. Smith. 2015. Selective electrochemical reduction of CO₂ to CO on CuO-derived Cu nanowires. *Physical Chemistry Chemical Physics: PCCP* 17: 20861–20867. doi:[10.1039/C5CP03559G](https://doi.org/10.1039/C5CP03559G).
56. Zhang, W., X. Wen, S. Yang, Y. Berta, and Z.L. Wang. 2003. Single-crystalline scroll-type nanotube arrays of copper hydroxide synthesized at room temperature. *Advanced Materials* 15: 822–825. doi:[10.1002/adma.200304840](https://doi.org/10.1002/adma.200304840).
57. Lin, C., Y. Lai, D. Mersch, and E. Reisner. 2012. Cu₂O/NiOx nanocomposite as an inexpensive photocathode in photoelectrochemical water splitting. *Chemical Science* 3: 3482–3487. doi:[10.1039/c2sc20874a](https://doi.org/10.1039/c2sc20874a).
58. Raciti, D., K.J. Livi, and C. Wang. 2015. Highly dense Cu nanowires for low-overpotential CO₂ reduction. *Nano Letters* 15: 6829–6835. doi:[10.1021/acs.nanolett.5b03298](https://doi.org/10.1021/acs.nanolett.5b03298).
59. Ma, M., K. Djanashvili, and W.A. Smith. 2016. Controllable hydrocarbon formation from the electrochemical reduction of CO₂ over Cu nanowire arrays. *Angewandte Chemie International Edition* 55: 6680–6684. doi:[10.1002/anie.201601282](https://doi.org/10.1002/anie.201601282).
60. Verdaguer-Casadevall, A., C.W. Li, T.P. Johansson, S.B. Scott, J.T. McKeown, M. Kumar, I. E.L. Stephens, M.W. Kanan, and I. Chorkendorff. 2015. Probing the active surface sites for CO reduction on oxide-derived copper electrocatalysts. *Journal of the American Chemical Society* 137: 9808–9811. doi:[10.1021/jacs.5b06227](https://doi.org/10.1021/jacs.5b06227).
61. Feng, X., K. Jiang, S. Fan, and M.W. Kanan. 2015. Grain-boundary-dependent CO₂ electroreduction activity. *Journal of the American Chemical Society* 137: 4606–4609. doi:[10.1021/ja5130513](https://doi.org/10.1021/ja5130513).
62. Lee, C.H., and M.W. Kanan. 2015. Controlling H⁺ vs CO₂ reduction selectivity on Pb electrodes. *ACS Catalysis* 5: 465–469. doi:[10.1021/cs5017672](https://doi.org/10.1021/cs5017672).
63. Ma, M., B.J. Trześniewski, J. Xie, and W.A. Smith. 2016. Selective and efficient reduction of carbon dioxide to carbon monoxide on oxide-derived nanostructured silver electrocatalysts. *Angewandte Chemie International Edition* 55: 9748–9752. doi:[10.1002/anie.201604654](https://doi.org/10.1002/anie.201604654).
64. Jia, F., X. Yu, and L. Zhang. 2014. Enhanced selectivity for the electrochemical reduction of CO₂ to alcohols in aqueous solution with nanostructured Cu-Au alloy as catalyst. *Journal of Power Sources* 252: 85–89. doi:[10.1016/j.jpowsour.2013.12.002](https://doi.org/10.1016/j.jpowsour.2013.12.002).
65. Kim, D., J. Resasco, Y. Yu, A.M. Asiri, and P. Yang. 2014. Synergistic geometric and electronic effects for electrochemical reduction of carbon dioxide using gold–copper bimetallic nanoparticles. *Nature Communications* 5: 4948. doi:[10.1038/ncomms5948](https://doi.org/10.1038/ncomms5948).
66. Siahrostami, S., A. Verdaguer-Casadevall, M. Karamad, D. Deiana, P. Malacrida, B. Wickman, M. Escudero-Escribano, E.A. Paoli, R. Frydendal, T.W. Hansen, I. Chorkendorff, I.E.L. Stephens, and J. Rossmeisl. 2013. Enabling direct H₂O₂ production through rational electrocatalyst design. *Nature Materials* 12: 1137–1143. doi:[10.1038/nmat3795](https://doi.org/10.1038/nmat3795).
67. Rasul, S., D.H. Anjum, A. Jedidi, Y. Minenkov, L. Cavallo, and K. Takanebe. 2015. A highly selective copper-indium bimetallic electrocatalyst for the electrochemical reduction of

- aqueous CO₂ to CO. *Angewandte Chemie International Edition* 54: 2146–2150. doi:[10.1002/anie.201410233](https://doi.org/10.1002/anie.201410233).
68. Sarfraz, S., A.T. Garcia-Esparza, A. Jedidi, L. Cavallo, and K. Takanebe. 2016. Cu–Sn bimetallic catalyst for selective aqueous electroreduction of CO₂ to CO. *ACS Catalysis* 6: 2842–2851. doi:[10.1021/acscatal.6b00269](https://doi.org/10.1021/acscatal.6b00269).
 69. Li, M., J. Wang, P. Li, K. Chang, C. Li, T. Wang, B. Jiang, H. Zhang, H. Liu, Y. Yamauchi, N. Umezawa, and J. Ye. 2016. Mesoporous palladium–copper bimetallic electrodes for selective electrocatalytic reduction of aqueous CO₂ to CO. *Journal of Materials Chemistry A* 4: 4776–4782. doi:[10.1039/C6TA00487C](https://doi.org/10.1039/C6TA00487C).
 70. Kortlever, R., I. Peters, S. Koper, and M.T.M. Koper. 2015. Electrochemical CO₂ reduction to formic acid at low overpotential and with high faradaic efficiency on carbon-supported bimetallic Pd–Pt nanoparticles. *ACS Catalysis* 5: 3916–3923. doi:[10.1021/acscatal.5b00602](https://doi.org/10.1021/acscatal.5b00602).
 71. Robertson, J. 2002. Diamond-like amorphous carbon. *Materials Science and Engineering: R: Reports* 37: 129–281. doi:[10.1016/S0927-796X\(02\)00005-0](https://doi.org/10.1016/S0927-796X(02)00005-0).
 72. Iijima, S. 1991. Helical microtubules of graphitic carbon. *Nature* 354: 56–58. doi:[10.1038/354056a0](https://doi.org/10.1038/354056a0).
 73. Zhu, H., J. Wei, K. Wang, and D. Wu. 2009. Applications of carbon materials in photovoltaic solar cells. *Solar Energy Materials and Solar Cells* 93: 1461–1470. doi:[10.1016/j.solmat.2009.04.006](https://doi.org/10.1016/j.solmat.2009.04.006).
 74. Kumar, B., M. Asadi, D. Pisasale, S. Sinha-Ray, B.A. Rosen, R. Haasch, J. Abiade, A.L. Yarin, and A. Salehi-Khojin. 2013. Renewable and metal-free carbon nanofibre catalysts for carbon dioxide reduction. *Nature Communications* 4: 2819. doi:[10.1038/ncomms3819](https://doi.org/10.1038/ncomms3819).
 75. Zhang, S., P. Kang, S. Ubnoske, M.K. Brennaman, N. Song, R.L. House, J.T. Glass, and T. J. Meyer. 2014. Polyethylenimine-enhanced electrocatalytic reduction of CO₂ to formate at nitrogen-doped carbon nanomaterials. *Journal of the American Chemical Society* 136: 7845–7848. doi:[10.1021/ja5031529](https://doi.org/10.1021/ja5031529).
 76. Wu, J., R.M. Yadav, M. Liu, P.P. Sharma, C.S. Tiwary, L. Ma, X. Zou, X.-D. Zhou, B.I. Yakobson, J. Lou, and P.M. Ajayan. Achieving highly efficient, selective, and stable CO₂ reduction on nitrogen-doped carbon nanotubes. *ACS Nano* 150423123413002. doi:[10.1021/acsnano.5b01079](https://doi.org/10.1021/acsnano.5b01079).
 77. Wu, J., M. Liu, P.P. Sharma, R.M. Yadav, L. Ma, Y. Yang, X. Zou, X.-D. Zhou, R. Vajtai, B. I. Yakobson, J. Lou, and P.M. Ajayan. 2016. Incorporation of nitrogen defects for efficient reduction of CO₂ via two-electron pathway on three-dimensional graphene foam. *Nano Letters* 16: 466–470. doi:[10.1021/acs.nanolett.5b04123](https://doi.org/10.1021/acs.nanolett.5b04123).
 78. Liu, Y., S. Chen, X. Quan, and H. Yu. 2015. Efficient electrochemical reduction of carbon dioxide to acetate on nitrogen-doped nanodiamond. *Journal of the American Chemical Society* 137: 11631–11636. doi:[10.1021/jacs.5b02975](https://doi.org/10.1021/jacs.5b02975).